Chapter 10

Fronts, Jet Streams and the Tropopause

M. A. Shapiro
NOAA/ERL/Wave Propagation Laboratory, Boulder, CO 80303

and

Daniel Keyser
Department of Atmospheric Science, State University of New York at Albany, Albany, NY 12222

10.1 Introduction

The advent of kite and balloon-borne meteorograph soundings during the early 1900s and the subsequent deployment of regional rawinsonde networks provided the observational basis for the study of the spatial and temporal evolution of fronts, jet streams and the tropopause. During the mid-century years (1935–1965), researchers focused on the structural characteristics of fronts and their associated jet streams near the tropopause, and on the diagnosis of the frontogenetic processes and secondary circulations governing their life cycles. The pioneering observational study by J. Bjerknes and E. Palmén (1937) showed fronts to be transitional zones of finite width (~100 km) and depth (~1 km), rather than near zero-order discontinuities extending from the surface to the tropopause. Newton (1954) presented the most comprehensive diagnosis of all components of upper-level frontogenesis during this period, and Sawyer (1956) and Eliassen (1962) derived the diagnostic theory for geostrophically forced secondary circulations about fronts based on the semigeostrophic equations, which was later expanded to the temporal dimension by Hoskins (1971) and Hoskins and Bretherton (1972).

In contrast to their upper-level counterparts, surface fronts received less attention from researchers during the period, with the exception of the classic study by Sanders (1955). The conceptual model of surface fronts and their evolution during the life cycle of extratropical cyclones

proposed by J. Bjerknes (1919) and J. Bjerknes and H. Solberg (1921, 1922), referred to as the Norwegian frontal cyclone model, received such wide acceptance that it remained virtually unaltered from the time of its inception.

In this chapter, the authors have chosen to review past and present interpretations that have arisen regarding the structure and governing dynamics of fronts, jet streams and the tropopause. It will be shown that new insights and the resolution of previous controversies have been linked, in part, to technological advances in atmospheric observing systems and, more recently, to the utilization of computers for diagnosis and numerical simulation.

For a historical review of fronts, jet streams and the tropopause, readers are referred to the works of Reiter (1975), Palmén and Newton (1969), Kutzbach (1979) and Keyser and Shapiro (1986). Recent advances in the study of surface and upper-level fronts are summarized by Reed in Sections 3.3.1 and 3.3.2 of this volume.

10.2 The Structure and Dynamics of Upper-Level Fronts, Jet Streams and the Tropopause

10.2.1 Structure

The study of the structure of upper-level fronts, associated jet streams and their relationship to the tropopause has resulted in significant differences in interpretation among researchers. Since the earliest frontal-tropopause model by J. Bjerknes (1932), several models have been proposed to describe the structure of fronts and jet streams in the vicinity of the tropopause (Fig. 10.1). These differences in interpretation stem from the limited availability of upper-air observations in regions of large horizontal gradients in tropopause height across jet streams at the level of maximum wind speed (LMW) (minimum horizontal thermal gradient). In reviews by Reed and Danielsen (1959), Shapiro (1976) and Keyser and Shapiro (1986), Berggren (1952) was cited for proposing a frontal-tropopause model in which the upper front was extended vertically through the "break" between the polar and subtropical tropopause and into the stratosphere above (Figs. 10.1d and 10.2). It has since been recognized that this structural concept was presented earlier by Nyberg and Palmén (1942). Nevertheless, Berggren (1952) is to be credited with utilizing closely spaced wind soundings to describe one example (Fig. 10.2) of ~100 km scale cyclonic wind shear within the vertical portion of an upper-level front at the LMW. Following its inception, the Nyberg–Palmén–Berggren model received limited acceptance, as there was considerable skepticism regarding the notion of vertically oriented fronts near the tropopause, defined by wind-only discontinuities, and the existence of air-mass and frontal discontinuities within the stratosphere. The deployment of meteorologically instrumented high-altitude (> 11 km) aircraft contributed to the resolution of the representativeness of the differing interpretations of frontal discontinuities near the tropopause. Studies based upon this new observing technology provided near-continuous horizontal and vertical profiles of wind velocity, temperature, turbulence and trace constituents (e.g., Shapiro 1974, 1976, 1978, 1980) which clearly

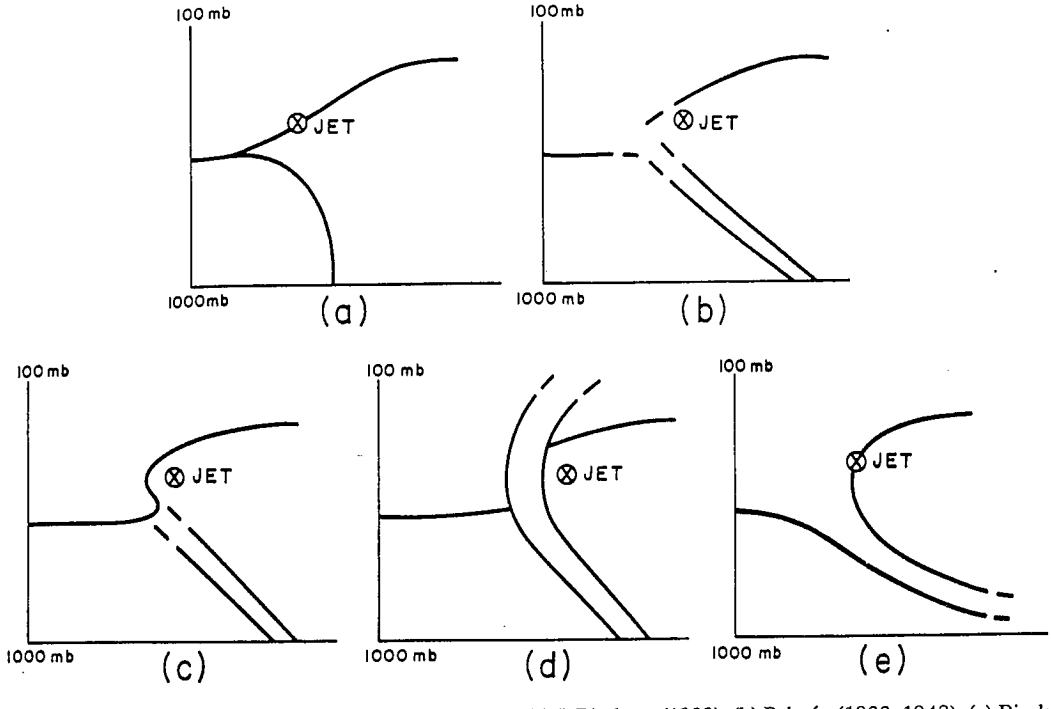

FIG. 10.1. Conceptual models of fronts in the vicinity of the tropopause: (a) J. Bjerknes (1932); (b) Palmén (1933, 1948); (c) Bjerknes and Palmén (1937); (d) Nyberg and Palmén (1942) and Berggren (1952); (e) Newton (1954) and Reed and Danielsen (1959).

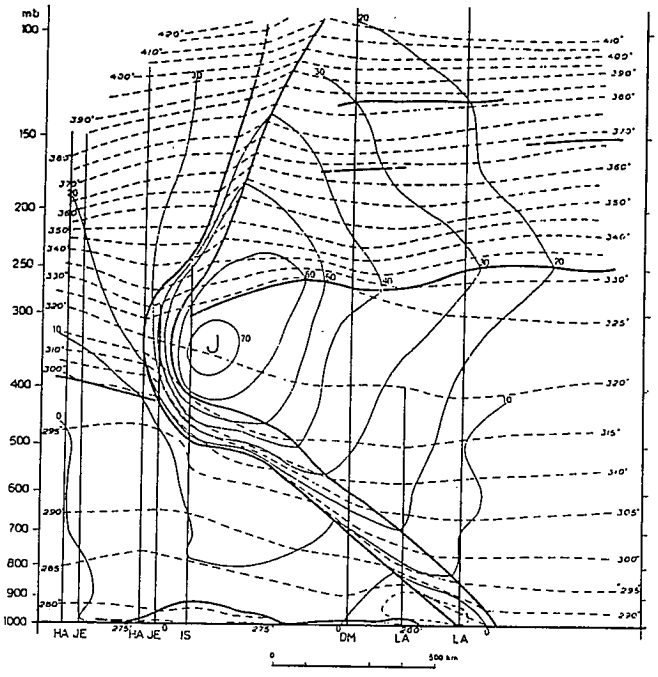

FIG. 10.2. Cross-section analysis of potential temperature (K, dashed lines), wind speed (m s^{-1}, thin solid lines), and frontal boundaries and the tropopause (heavy solid lines) (Berggren 1952).

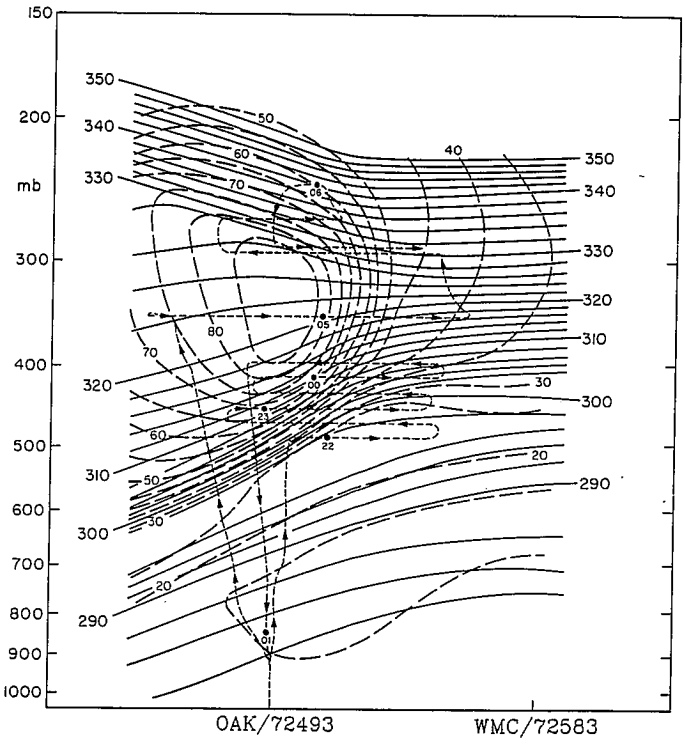

FIG. 10.3. Composite cross-section analysis for ~00 UTC 16 April 1976 of potential temperature (K, solid lines), wind speed (m s^{-1}, heavy dashed lines), and NCAR Sabreliner aircraft flight track (thin dashed lines, time marks at solid dots, UTC) (Shapiro 1978).

described the ~100-km scale in frontal cyclonic wind speed shear at the LMW (Fig. 10.3). Subsequent measurements with a NASA RB-57F stratospheric aircraft (Shapiro et al. 1980) documented the stratospheric extension of frontal-scale transitions in potential vorticity and ozone to above 100 mb (16 km), verifying the stratospheric air-mass structure proposed by Nyberg, Palmén and Berggren.

Frontal layers have been identified by their discontinuities in horizontal thermal gradient, static stability, lateral and/or vertical wind velocity gradients and potential vorticity (Palmén 1948). The equations defining the physical processes governing the generation and decay of frontal gradients derived by Miller (1948) formed the basis for numerous frontal diagnostic studies (e.g., Reed and Sanders 1953; Newton 1954; Bosart 1970). The individual Miller frontal parameters (e.g., horizontal and vertical gradients of temperature and wind velocity), however, did not show discontinuities throughout the entire frontal domain, leading to questions on the definition of fronts near the tropopause. Consider Fig. 10.4, which illustrates one such jet-front system. Figure 10.4a shows a frontal layer in the troposphere beneath a polar jet-stream core bounded by discontinuities in the horizontal and vertical gradients of potential temperature and wind velocity. Similar discontinuities bound the sloping baroclinic layer within the stratosphere above the jet-stream core. A ~100-km wide frontal region, continuous with the sloping frontal layers above and below and containing large cyclonic wind shear, is situated within the polar stratosphere at the LMW where discontinuities in the horizontal and vertical gradients of potential temperature vanish. Nyberg and Palmén (1942), Berggren (1952) and Shapiro (1976) termed "frontal" the total jet-stream region which contains hypergradients in either or both wind velocity and potential temperature.

Kleinschmidt (1951) was the first to use isentropic potential vorticity and its discontinuities to define the stratosphere and its interface with the troposphere (the tropopause). In later studies, Reed (1955) and Reed and Danielsen (1959) utilized potential vorticity and its spatial discontinuities (see Fig. 3.9) to establish the dynamical relationship between the folding of the tropopause and upper-level frontogenesis. Although discontinuities in potential vorticity (Fig. 10.4b) bound the mesoscale wind velocity gradients in the layer of maximum wind (see Shapiro 1976, 1978) and define the approximate separation of air of stratospheric versus tropospheric origin, they do not delineate frontal discontinuities in the middle troposphere. In that region, potential vorticity and its discontinuities tend to vanish, as the relative vorticity on isentropic surfaces becomes weakly anticyclonic (see Figs. 10.4a and d). Thus, taken individually, discontinuities in potential temperature, vertical and horizontal wind shear, and potential vorticity do not uniquely define the total frontal domain of upper-level jet-front systems. It remained for future research to define a unifying parameter describing the total frontal domain.

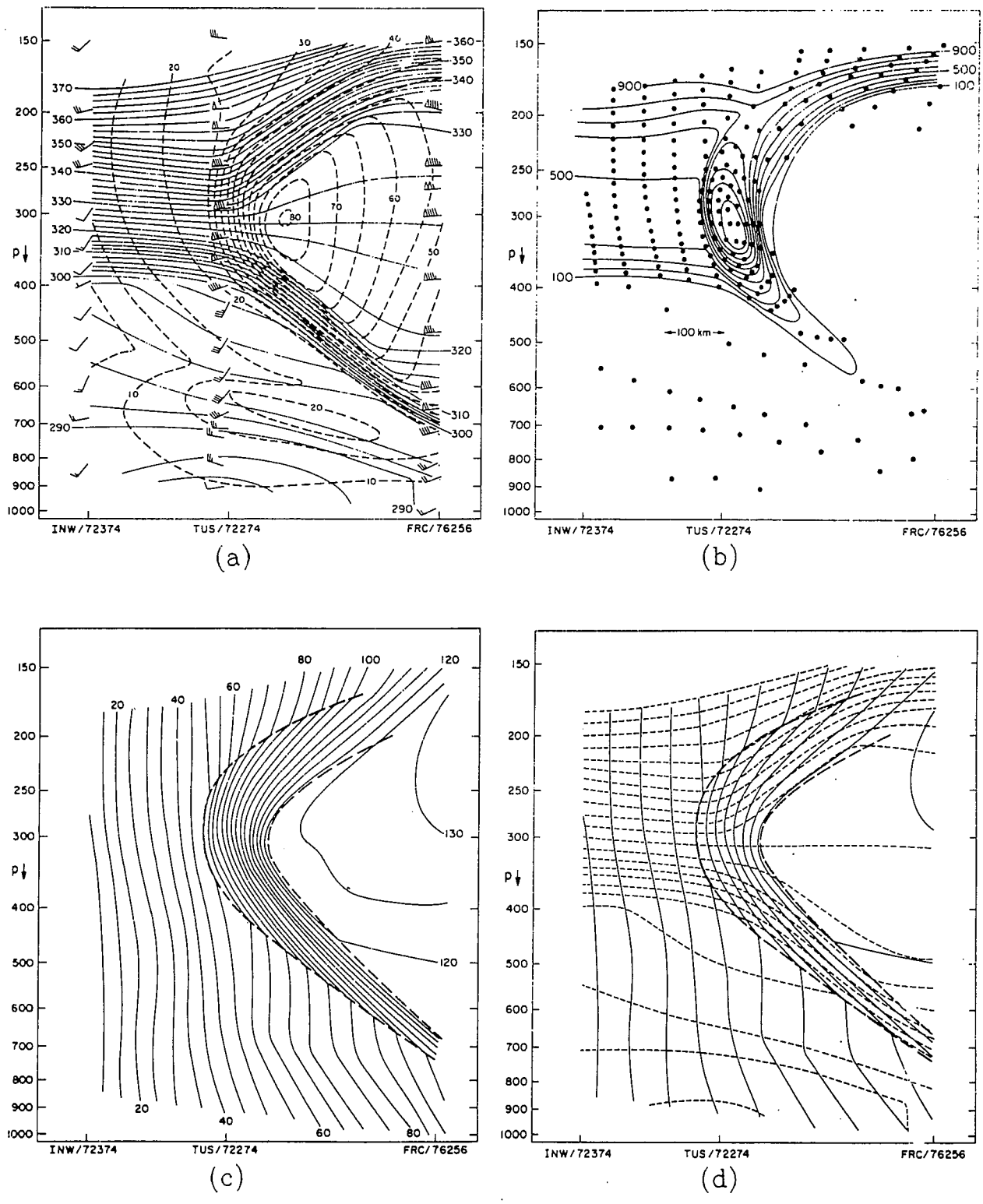

FIG. 10.4. Cross sections for 00 UTC 17 April 1976 based on rawinsonde observations at Winslow, Arizona (INW), Tucson, Arizona (TUS), and Guaymas, Mexico (FRC), supplemented with NCAR Sabreliner aircraft data in the layer between 250 and 300 mb: (a) Potential temperature (K, solid lines) and wind speed (m s^{-1}, dashed lines). In this and all ensuing figures, winds are plotted with respect to north at the top of the figure; flags, full barbs and half barbs, respectively, indicate speeds of 25, 5 and 2.5 m s^{-1}. (b) Potential vorticity (10^{-7} K mb^{-1} s^{-1}, solid lines) and array of dots formed by the intersection of (M, θ) coordinates displayed in panel (d). (c) Absolute momentum, $M = U - fy$ (m s^{-1}, solid lines), with y=0 at left side of figure, decreasing toward the right. (d) (M, θ) coordinate grid from patterns in panels (a) and (c), with contour intervals of 10 m s^{-1} and 4 K. Heavy dashed lines in (c) and (d) indicate first-order discontinuities in M (Shapiro 1981).

Eliassen (1952) introduced the concept of absolute angular momentum (see Section 9.2) in describing forced secondary circulations about an axially-symmetric circumpolar vortex. In later studies, Eliassen (1959, 1962) defined the Cartesian reference frame analogy as absolute momentum, i.e.,

$$M = U - fy, \tag{10.1}$$

where U is the along-front component of geostrophic velocity, f the Coriolis parameter and y the horizontal distance in the cross-front direction (positive toward colder air).

The cross-front vector vorticity $\mathbf{q}$ is

$$\mathbf{q} = -\mathbf{k}\frac{\partial M}{\partial y} - \mathbf{j}\frac{\partial M}{\partial p}, \tag{10.2}$$

with the orientation of $\mathbf{q}$ directed along the vortex lines, i.e., along isopleths of constant M, where $-\partial M/\partial y$ and $-\partial M/\partial p$ are the respective vertical and horizontal components of $\mathbf{q}$. Shapiro (1981) evaluated the distribution of absolute momentum for cases of well-developed upper-level jet-front systems. The results (Fig. 10.4c) revealed that the total hypergradient region of jet-front systems is bounded by discontinuities in the horizontal and/or vertical gradient of absolute momentum. Thus, it was suggested that absolute momentum and its spatial discontinuities be used to define the total hypergradient region of jet stream–frontal zone systems. Figure 10.4d shows the superposition of isopleths of absolute momentum and potential temperature. For adiabatic, inviscid motions, air parcels conserve potential temperature, and changes in their absolute momentum arise from cross-front geostrophic flow ($dM/dt = -fV_g$). The reference frame composed of the (M, θ) lines forms a stretched Lagrangian coordinate grid, where the horizontal distortion of M lines away from the equally spaced Cartesian y lines is proportional to the vertical component of the vector vorticity. An (M, p) type of coordinate system was used by Hoskins (1971) and Hoskins and Bretherton (1972) for their analytical solutions of semigeostrophic frontogenesis (see Section 9.8).

Conceptual models describing the meridional (pole-to-equator) structure of the tropopause and the positioning of the principal jet streams and frontal zones have also evolved in response to new observational technologies. The research-aircraft-based studies by Shapiro (1985) and Shapiro et al. (1987) presented analyses describing anew the arctic tropopause, jet stream and frontal structure in association with high-latitude polar vortices. The arctic jet stream was found north of the polar jet with well-defined potential vorticity tropopause folds between the lower (~5 km) arctic tropopause to the north and the higher (~7 km) polar tropopause to the south. Earlier models of the key jet streams and tropopause surfaces (e.g., Palmén 1951; Defant and Taba 1957; Palmén and Newton 1969, Fig. 4.7) did not include the arctic jet stream or a low (~5 km) arctic tropopause at high latitudes, nor did they explicitly include the potential vorticity discontinuity between the stratosphere and troposphere and its folding characteristics.

Figure 10.5 presents a revised meridional model of the tropopause, primary jet streams and fronts from Shapiro et al. (1987). The tropopause is defined by the stratospheric-tropospheric potential vorticity discontinuity, and

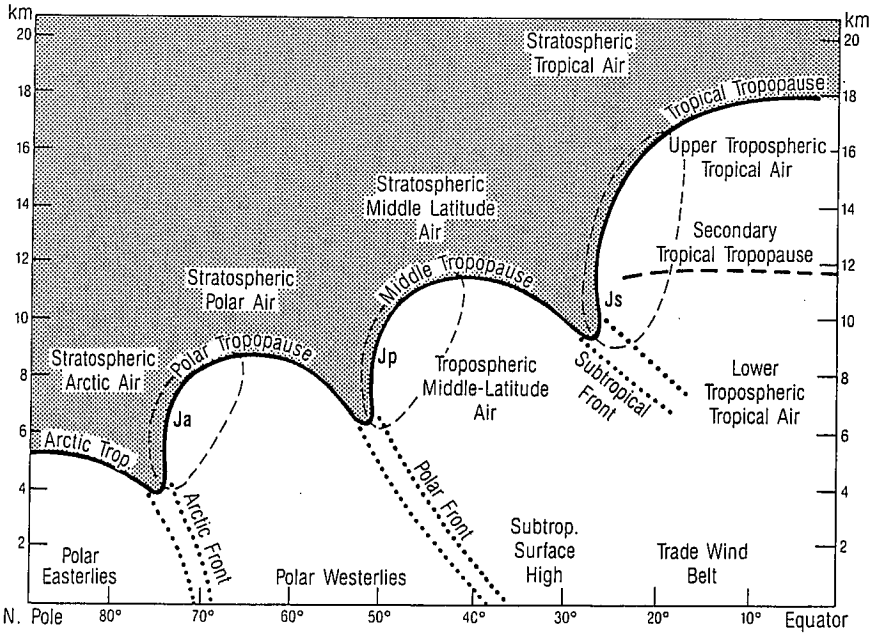

FIG. 10.5. The meridional structure of the tropopause. Potential-vorticity-discontinuity tropopause: heavy solid lines, with stratosphere stippled. The primary frontal zones are bounded by the heavy dotted lines and are labeled accordingly. The 40 m s^{-1} isotach (thin dashed line) encircles the cores of the three primary jet streams: arctic, Ja; polar, Jp; and subtropical, Js. The secondary (thermal) tropical tropopause is indicated by the heavy dashed line. Major tropospheric and stratospheric air masses, tropopause surfaces, and selected wind systems are labeled in the cross section. Individual cross sections may differ spatially and temporally from that presented in this idealized meridional model (Shapiro et al. 1987).

(with this convention) is continuous from pole to equator. It is not a material interface between the stratosphere and troposphere, as stratospheric-tropospheric exchange of air and trace constituents is accomplished through potential-vorticity-altering processes. These range from seasonal radiative processes (e.g., Reiter 1975) to episodic events such as turbulent mixing within tropopause folds (e.g., Shapiro 1978, 1980) and penetrative mesoconvective cloud systems. Three jet streams and their associated tropopause folds are shown in the schematic: the arctic jet (Ja) at 70°N, the polar jet (Jp) at 45°N and the subtropical (Js) jet at 25°N. As in Palmén and Newton's figure, the secondary tropical tropopause at 12 km is shown below the primary tropical tropopause at 18 km. The subtropical jet stream tropopause fold, however, is drawn continuous with the tropical tropopause at 18 km because of the low potential vorticity of the upper-tropospheric tropical air south (anticyclonic shear side) of the subtropical jet in the layer bounded vertically by the primary and secondary tropical tropopause surfaces. With the exception of the addition of the arctic jet stream and the tropopause defined in terms of the potential vorticity, all other primary wind systems and air masses are as in the Palmén and Newton (1969, Fig. 4.7) cross section.

The meridional structure of the tropopause and the position and intensity of the primary wind systems and fronts depicted in Fig. 10.5 can vary considerably, both spatially and temporally. In the extreme, one or more of the primary jet streams and their associated fronts and tropopause folds may not be present in a given cross section on any given day. On occasion, two jet-front systems (i.e., the arctic and polar, or the polar and subtropical) will merge into a single jet-front system, such that roughly half of the midtropospheric pole-to-equator baroclinicity is concentrated within a frontal zone of ~200 km width. Finally, zonally- or seasonally-averaged meridional cross sections would only contain the subtropical jet (Fig. 2.2), and a broad general slope of the mean potential vorticity isopleths (Fig. 5.5) rather than distinct tropopause folds, owing to the localized (spatial) and transient (temporal) character of the polar and arctic jet streams.

10.2.2 Dynamics

The dynamics governing the evolution of fronts in the vicinity of the tropopause have been the focus of numerous investigations during the past half-century. During this period there arose differences in interpretation with regard to the key processes governing the evolution of these systems. The most controversial of the differing interpretations centered on the sense of the transverse (cross-front) secondary circulation associated with the contraction of upper-tropospheric frontal gradients. On the one hand, Namias and Clapp (1949), acknowledging a conception by R. C. Sutcliffe, were the first to discuss the thermally direct circulation relative to the jet stream forced by a confluent geostrophic deformation (Fig. 10.6a). Ascending and descending air currents were found to the warm and cold sides of the upper-level baroclinic zone, respectively. These diagnostically derived circulations were treated theoretically and/or numerically by Sawyer (1956), Eliassen (1962), Hoskins and Bretherton (1972), Gidel and Shapiro (1979), and Keyser and Pecnick (1985a,b).

Another interpretation of the transverse circulations during upper-level frontogenesis was discussed by Reed and Sanders (1953), Newton (1954), Bosart (1970) and Shapiro (1970). These synoptic studies provided evidence for strong sinking motions within and to the warm side of developing upper fronts, concluding that upper-level frontogenesis was predominantly forced by cross-front differential vertical motions in the thermally indirect sense, acting to increase frontal thermal gradients and vorticity. Newton (1954) stressed that upper-level frontogenesis was a three-dimensional process which did not lend itself to the two-dimensionalization of the Namias and Clapp (1949) confluence theory, as large-scale horizontal deformations associated with evolving upper-tropospheric synoptic waves are more complex than a simple two-dimensional cross-front geostrophic confluence, independent of height, in a straight geostrophic current. Support for the apparent necessity of the three-dimensional treatment of upper fronts came from studies such as those of Mudrick (1974), Shapiro (1975) and Newton and Trevisan (1984a,b), wherein three-dimensional primitive equation numerical

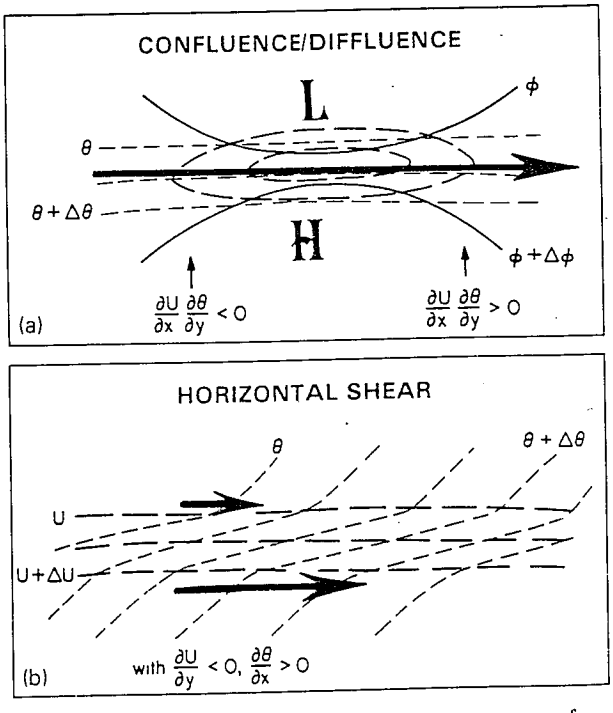

FIG. 10.6. Schematic depictions on a constant pressure surface, of straight frontal zones characterized by (a) confluence and diffluence associated with a jet maximum, and (b) horizontal shear in the presence of a positive along-front thermal gradient. Geopotential height contours, thick solid lines; isotachs of the along-front geostrophic wind component U, thick dashed lines; isentropes, thin dashed lines. Heavy arrows indicate the jet axis in (a) and the sense of cross-front shear of the along-front wind component in (b) (adapted from Shapiro 1982).

simulations produced upper-level frontogenesis, tropopause folding and strong sinking motion at the warm side of the frontal layer, in agreement with the interpretation of the three-dimensional synoptic studies.

The differences in interpretation regarding the sense of the secondary circulations about upper fronts were considered by Shapiro (1981), Keyser and Pecnick (1985a,b) and Reeder and Keyser (1988). Shapiro's (1981) observational study utilized the Sawyer-Eliassen secondary circulation equation, (9.20) in Section 9.3, to show the importance of the previously neglected cross-front horizontal wind shear acting upon along-front thermal gradients (Fig. 10.6b), in addition to cross-front confluence (Fig. 10.6a), in forcing strong sinking motion within and to the warm side of intensifying upper fronts (see Fig. 9.7). Keyser and Pecnick (1985a,b) and Reeder and Keyser (1988) applied a two-dimensional (cross-front) numerical simulation model to study the interplay between geostrophic confluence and cross-frontal geostrophic wind shear acting upon cross-front and along-front thermal gradients, respectively. The results from these studies showed that the effect of horizontal shear upon a positive along-front thermal gradient (cold-air advection) was to displace the thermally direct circulation toward the warm side of developing upper-level fronts (Fig. 10.7). The shift in the position of the axis of the secondary circulation yielded sinking motion which was strongest at the warm side of the front. Thus, the cross-frontal gradient in vertical motion was frontogenetical and had the local appearance of being thermally indirect, while the overall secondary circulation was in the kinetic-energy-generating thermally direct sense as required for the development and maintenance of upper-level jet streams.

The relationship of the forcing of upper-level jet-front secondary circulations to the character of the synoptic-scale flow is illustrated in Fig. 10.8. The schematic shows geostrophic confluence (diffluence) in the entrance (exit) of the jet-front as it propagates through the synoptic wave. In contrast, the thermal advections along the frontal zone range from zero in the pure confluence (diffluence) case (Fig. 10.8a) to cold and warm air advection as the jet-front passes from the northwesterly to the southwesterly wave inflections (Fig. 10.8b and d, respectively). The effect of the cross-jet cyclonic and anticyclonic wind shears upon the varying along-front thermal gradients is to force a variety of cross-front secondary circulations differing from the simplified pure confluent (diffluent) straight-jet secondary circulation (see Keyser and Pecnick 1985a). It is now apparent, in retrospect, that differences in interpretation of upper-level jet-front secondary circulations resulted in part from consideration of these systems during various stages of their life cycles.

10.3 The Scale Contraction of Surface Fronts and its Role in the Initiation of Mesoconvective Precipitation Systems

10.3.1 Frontal Contraction

In reviewing the earlier concepts of surface fronts, one finds that fronts near the ground were first considered to be zero-order discontinuities in density (temperature) and wind velocity between air masses of different origin. The early studies (reviewed by Bergeron 1959) documented the abrupt change in wind direction and the temperature decrease during cold frontal passage. The accompanying

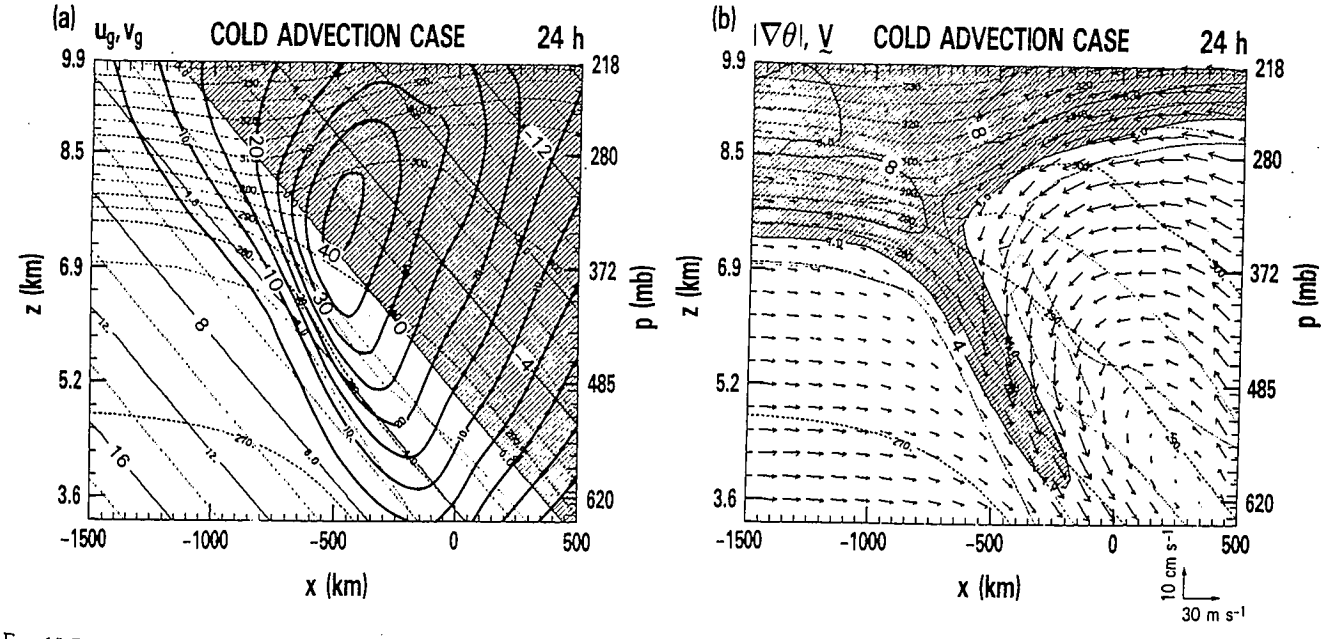

FIG. 10.7. Cross sections at 24 h from a two-dimensional primitive equation model of frontogenesis incorporating horizontal shear: (a) Cross-front geostrophic component u_g (contour interval 2 m s^{-1}, thin solid, negative values shaded) and along-front geostrophic component v_g (interval 5 m s^{-1}, thick solid); (b) $|\Delta\theta|$ [contour interval 2 K (100 km)$^{-1}$, thin solid, values $>$ 4 shaded] and vector arrows of the total flow in the cross-front plane (u,w). Background field is potential temperature (interval 5 K, dashed) (Keyser et al. 1986).

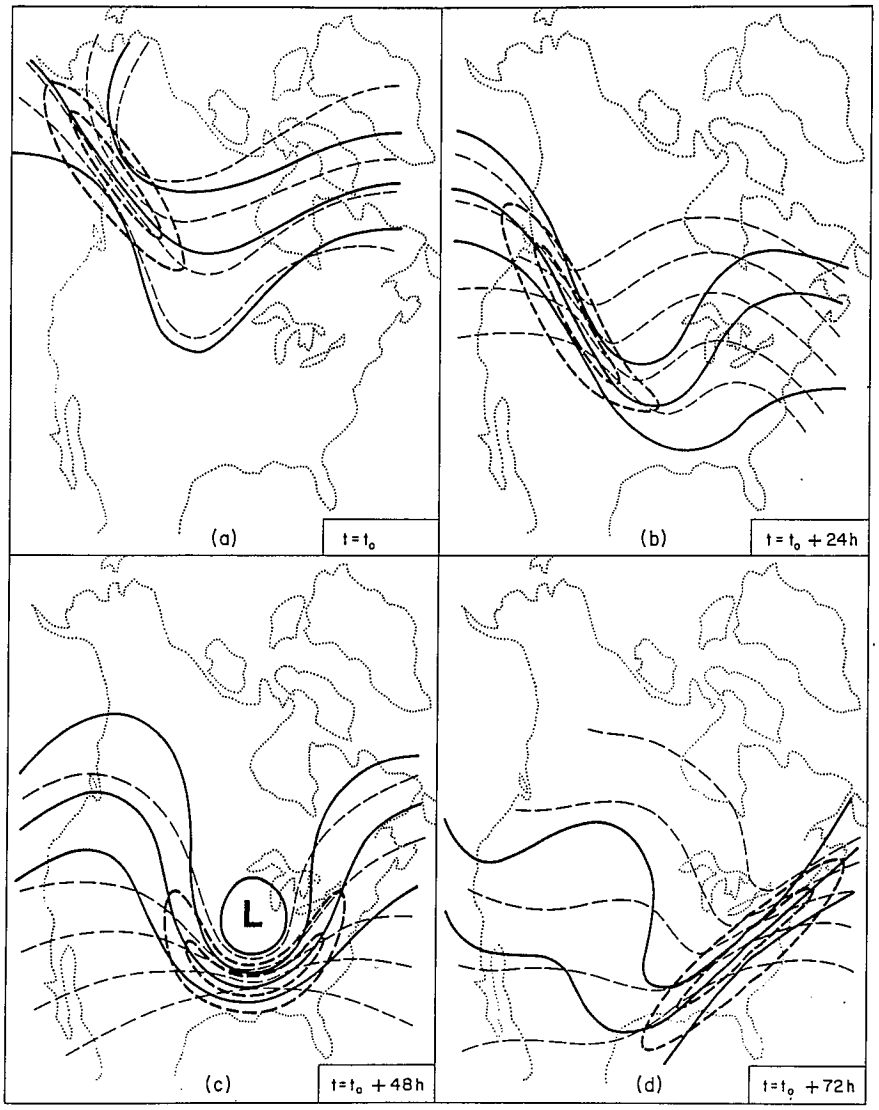

FIG. 10.8. Idealized schematic depiction on a constant pressure surface of the propagation of an upper-tropospheric jet-front system through a midlatitude baroclinic wave over a 72-h period: (a) formation of jet-front in the confluence between mid- and high-latitude currents; (b) jet-front situated in the northwesterly flow inflection of amplifying wave; (c) jet-front at the base of the trough of fully developed wave; (d) jet-front situated in the southwesterly flow inflection of damping wave. Geopotential height contours, thick solid lines; isotachs, thick dashed lines; isentropes or isotherms, thin dashed lines (Shapiro 1982).

theoretical treatments (e.g., Margules 1906) used laws of hydrodynamics applied to "two-density" fluid models containing a sloping frontal interface to describe the motion, slope and vertical circulations of fronts. With the advent of kite and balloon-borne upper-air observations, it was discovered that fronts aloft were actually transition zones of finite width having characteristic vertical and horizontal scales of ~1 km and ~100 km (Bjerknes and Palmén 1937). At this point, the concept of fronts as zero-order discontinuities within synoptic-scale (~1000 km) cyclones was de-emphasized. Fronts thereafter were treated as transition layers which, as demonstrated by Palmén (1948), are bounded by first-order discontinuities in temperature and velocity that are related to the slope of a front. It continued to be appreciated, however, that sharp horizontal discontinuities could exist on very small scales (0.2–2 km), such as at the outflow boundaries of convective precipitation systems, land-sea breeze convergence lines and orographically-forced flows (e.g., Charba 1974; Goff 1976; Simpson et al. 1977; Matthews 1981; Carbone 1982; Wakimoto 1982; Hobbs and Persson 1982).

We suggest that the shift from the discontinuous "wedge" (two-density) model to the continuous "zone" model resulted from combining synoptically spaced (~400 km) upper-air observations with the ~100 km spacing of the hourly reporting surface stations, along with the decline in the use of single-station (continuous record) analysis of frontal zones. Furthermore, with the expansion of synoptic observing networks and the introduction of the quasi-geostrophic theory, fronts were treated as synoptic-scale (~1000 km) in length, but mesoscale (~100-200 km) in width, with the narrow width resulting from the

contractions of synoptic-scale thermal gradients forced by geostrophic deformation and its ageostrophic circulation response.

Bergeron (1928) and Petterssen (1936) first described the deformation fields contributing to the contraction of temperature and velocity gradients into narrow surface frontal zones. Since then, the importance of geostrophic deformation and its coupled vertical secondary circulations has been examined in frontal studies by Sawyer (1956), Eliassen (1959, 1962), Williams (1967) and Hoskins and Bretherton (1972), among others. Eliassen (1959) recognized that secondary circulations give rise to a "self-sharpening" process to accelerate the scale contraction of surface fronts. Williams (1967, 1972) and Hoskins and Bretherton (1972) simulated this process (ageostrophic contraction) through numerical and analytic solutions, respectively (see Section 9.8). In the absence of fine-scale turbulent motions, there are no limits to the scale to which frontal gradients may contract under the combined actions of geostrophic and ageostrophic motions. Inviscid, adiabatic, semigeostrophic frontogenesis theory produces infinitesimally narrow fronts within a finite time (Hoskins and Bretherton 1972). The finite vertical and horizontal scales of frontal zones are presumed to result from a balance between frontogenetical synoptic-scale forcing and frontolytical turbulent-scale mixing (e.g., Williams 1974). Accelerated frontal contractions transpire when latent heat release occurs within the ascending motion at the leading edge of fronts (e.g., Browning and Harrold 1970; Carbone 1982), after the frontal dynamics are modified by the effects of water vapor phase changes and nonhydrostatic pressure changes. Surface boundary-layer heat and momentum fluxes also contribute to vertical circulations about fronts (e.g., Keyser and Anthes 1982; Shapiro 1982; Koch 1984; Reeder 1986).

Recent observational studies with research aircraft, an instrumented 300-m tower and ground-based remote sensors have documented the cross-frontal scale collapse of the leading edge of nonprecipitating surface cold fronts down to horizontal distances of $\lesssim 1$ km (Shapiro 1984; Shapiro et al. 1985). The example from Shapiro et al. (Fig. 10.9a) shows the passage of a surface cold front by the NOAA/Boulder Atmospheric Observatory (BAO) instrumented 300-m tower. This front had the structural characteristics of a density current: an elevated hydraulic head followed by a turbulent wake. The cross-frontal scale was ~ 1 km and vertical motions at the frontal head exceeded 4 m s^{-1} (Fig. 10.9b). An acoustic sounder documented the structure of the frontal interface as it passed the BAO tower (Fig. 10.9c). Results from these observational studies initiated debate among researchers on the nature of the observed frontal scale collapse in the absence of precipitation processes, revived an earlier controversy regarding the role of "pressure jumps" at or in advance of surface fronts in triggering mesoconvective precipitation systems, and inspired numerical modelers to attempt simulating these structures using nonhydrostatic models (Gall et al. 1987, 1988).

The frontal scale collapse studies of Shapiro (1984) and Shapiro et al. (1985) were received with a degree of skep-

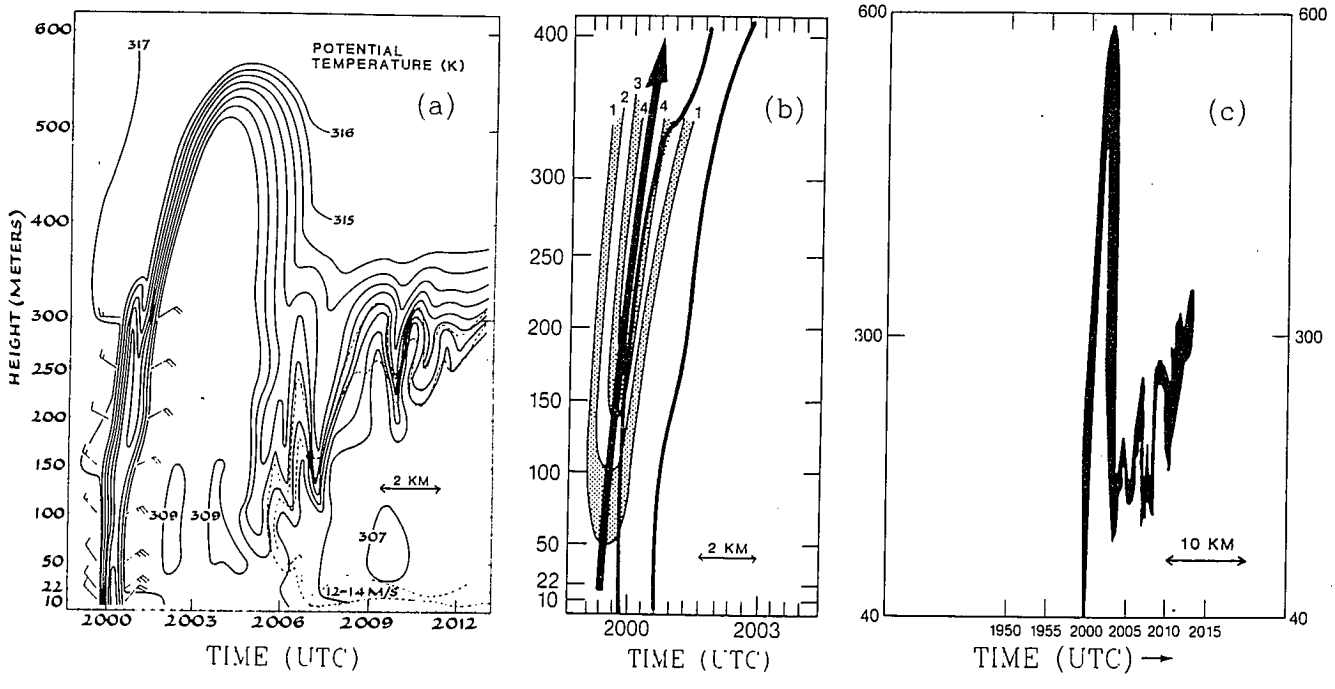

FIG. 10.9. Frontal passage at the BAO tower between 1959 and 2013 UTC 19 September 1983: (a) Potential temperature (K) derived from tower data up to 300 m and the acoustic record in panel (c) between 300 and 600 m. Region of the 12–14 m s^{-1} wind speed surge, stippled area; wind flags (full barb, 5 m s^{-1}) show tower winds preceding and following the passage of the front. (b) Vertical motion (m s^{-1}) at the leading edge of the front, whose boundaries are indicated by heavy solid lines. (c) Acoustic sounder record between 1950 and 2015 UTC, measured at the BAO tower (Shapiro et al. 1985).

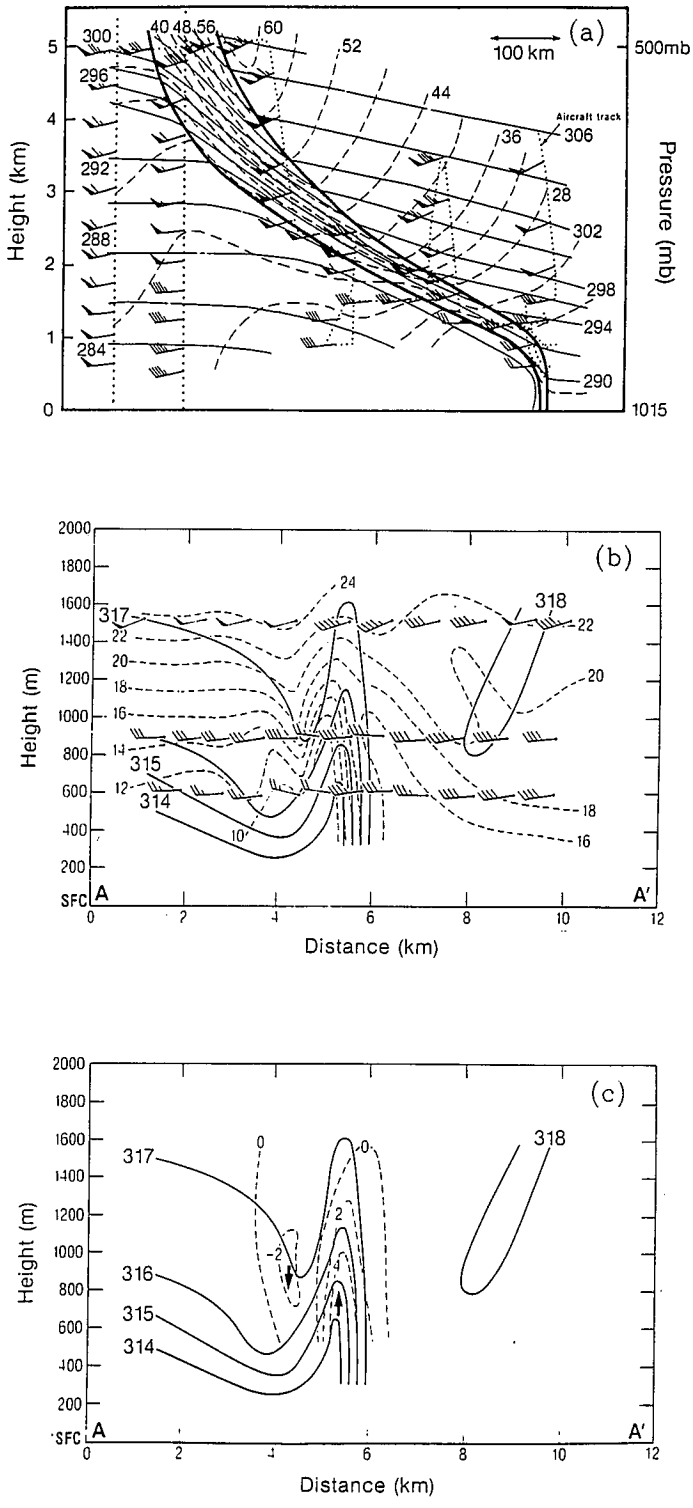

FIG. 10.10. (a) Cross section analysis of potential temperature (K, thin solid lines), along-front wind component (m s^{-1}, dashed lines) and frontal boundaries (heavy solid lines) for an eastern Pacific cold front at ~00 UTC 10 December 1987. NOAA P-3 aircraft flight track, dotted line; dropwindsonde profiles, heavy dotted lines and wind symbols. Left and right endpoints are 44.4°N, 135.3°W and 39.8°N, 130.6°W (cf. Fig. 10.11). (b) The leading edge of the cold front shown in (a) at ~03 UTC: potential temperature, front-parallel wind speed (dashed lines), and selected flight-level wind vectors. (c) Potential temperature and measured vertical velocity (m s^{-1}, dashed). See also Fig. 8.23.

ticism, as it was suggested that these extremely narrow fronts were a manifestation of the steep topography of the eastern slopes of the Rocky Mountains. Orlanski et al. (1985) regarded these observed narrow fronts as atypical, classifying them as orographically-trapped Kelvin waves forced by synoptic-scale fronts impinging on the eastern slopes of the mountains. What was required to resolve this concern was the documentation of such nonprecipitating frontal structure over flat terrain. This opportunity arose during the Ocean Storms 1987 field program, during which a NOAA P-3 research aircraft was used to document the horizontal (cross-frontal) scale of a frontal zone over the eastern Pacific Ocean. In this study, the aircraft was used to deploy dropwindsondes and was flown in a descending "stairstep" profile, tracing the front from the middle troposphere (~500 mb) down to the sea surface (Fig. 10.10a). The microscale structure of the leading edge of the front was observed in vertical profile (Fig. 10.10b), defining the narrow ~1 km frontal discontinuity. Note the ~5 m s^{-1} ascent at the leading edge of the front (Fig. 10.10c). The companion satellite image (Fig. 10.11) shows the "rope cloud" signature of the enhanced nonprecipitating cumulus band formed by the ascending motion at the leading edge of the front.

It is interesting to observe that interpretations of the transverse scale of surface cold fronts have come full circle. The earlier near zero-order discontinuity model was put aside only to be rediscovered using "modern" instrumentation.

10.3.2 Frontal-Mesoconvective Interaction

Fronts and their associated vertical circulations have long been recognized as a mechanism for lifting moist air to its level of free convection and initiating the release of potential instability through deep mesoconvective cloud systems. An alternative hypothesis for triggering prefrontal thunderstorms was proposed in the theoretical treatments of Freeman (1948) and Abdullah (1949), with extensive observational documentation by Tepper (1950). These studies proposed that frontal and prefrontal squall lines were initiated by hydraulic (nonhydrostatic) pressure waves or "jumps" on an inversion layer, generated by the horizontally accelerated motion of cold fronts. On occasion, these pressure jumps were thought to propagate out in advance of the triggering front. The documentation of these fine-scale phenomena by Tepper (1950) was based upon an automatic 55-station pressure, wind and temperature observing network with ~3-km spacing.

Newton (1950) questioned the applicability of the gravity wave as a triggering mechanism for warm-sector squall lines, noting that a great amount of lifting would be required for condensation in the ordinarily dry air above the inversion, whereas convection from the moist layer beneath would destroy the stable layer necessary for further propagation of the jump wave. Fujita (1955) argued and presented evidence that the pressure jump lines of Tepper (1950) were the result of, rather than the

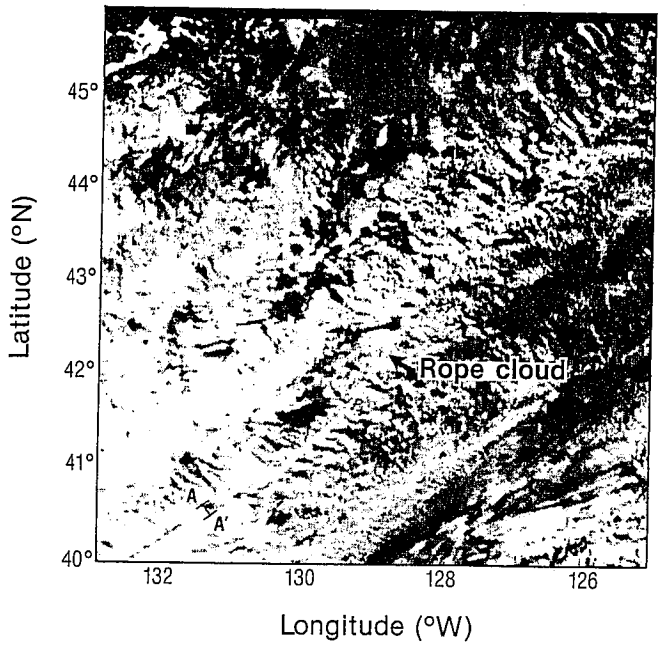

FIG. 10.11. 1-km resolution visible satellite image at 23 UTC 9 December 1987. Line AA′ (SW corner) indicates the front-relative projection line of Fig. 10.10b-c.

cause of, squall lines. We suggest that the limited acceptance of nonhydrostatic frontal phenomena as an initiation mechanism for mesoconvective systems was due in part to the lack of documentation of the vertical structure of the pressure jump lines. It is only recently that instrumented towers and research aircraft have provided some corroborating evidence for density-current (hydraulic-head) characteristics of surface cold fronts. The recent studies have shown examples where nonprecipitating fronts have assumed the characteristics of density-current flows. The large ascending vertical motions (~ 5 m s^{-1}) at the frontal head are of sufficient magnitude to lift potentially unstable air through the trapping "lid" inversions described by Carlson and Ludlam (1968) and Carlson et al. (1983), which often cap moist surface layers. The frontal head is capable of releasing the potential instability of trapped moist layers on time scales of minutes rather than hours, as would be required for the 20 cm s^{-1} lifting of ~100-km frontal-scale vertical circulations. It is not unreasonable to consider the possibility that the frontal head may separate itself from its parent front and propagate out in advance of the front as a solitary wave, as proposed by Abdullah (1949). The separation process could produce prefrontal pressure waves, as in Tepper (1950), and initiate precipitation systems in the prefrontal environment.

10.4 The Life Cycle of the Marine Extratropical Cyclone and its Fronts

Since its inception, the Norwegian cyclone model (J. Bjerknes 1919; Bjerknes and Solberg 1921, 1922) has formed the conceptual basis for describing the evolution of fronts during the life cycle of extratropical cyclones. Although this model was derived primarily from the analysis of eastern Atlantic Ocean and western European observations, it has been applied in a variety of flow regimes over land, sea and in the vicinity of steep topography. The vertical structure of fronts within this model was conceived from sparse meteorograph and kite soundings, surface observations taken along mountain slopes, and visual observations of differential motions between cloud layers situated at different altitudes above and below fronts. Quite cleverly, these early researchers deduced the three-dimensional thermal structure of cyclones, including the slopes of frontal layers and the vertical wind shear through them, from visually derived cloud-motion winds coupled with the geostrophic thermal wind relationship, in addition to detailed analyses of sea-level pressure and surface temperature observations.

Figure 10.12 presents the conceptual model of the Norwegian cyclone from J. Bjerknes and Solberg (1922). The schematic shows the amplification of the frontal wave from its incipient phase, through cyclogenesis, to its frontal occlusion. Note that the model includes a "seclusion" at the northern tip of the occluded front, denoting the entrapment of initially warm-sector air at the center of the cyclone (shown in Phase IV). This conceptualization included a description of the vertical structure of warm, cold and occluded fronts and their associated cloud and precipitation systems.

As researchers began explorations with the operational upper-air networks during the post-World War II years, the resulting studies revealed cyclone and frontal structure that did not always extend continuously from the surface to the tropopause as previously shown by Bjerknes and Palmén (1937). (See Figs. 3.3 and 9.1.) These new case studies emphasized the vertical separation and differing governing dynamics of upper-level versus lower-level (surface) fronts (e.g., Reed and Sanders 1953; Newton 1954; Sanders 1955; Bosart 1970; Shapiro 1970). It should be noted that these studies of the structural and dynamical separation of fronts near the tropopause from those near the ground were based exclusively on weather events over the central United States during situations of weak lower-tropospheric cyclogenesis, but strong upper-tropospheric synoptic wave amplification. Despite these differences in interpretation of the vertical structures of fronts from the earlier conceptual models, researchers and forecasters were hesitant to suggest significant alternatives to the Norwegian frontal-cyclone model.

The advent of electronic computers during the 1950s provided the technology with which to simulate and predict numerically the life cycles of synoptic-scale weather systems and their embedded mesoscale structures. The most recent advances in computational technology have led to the simulation of idealized and actual cyclogenetic events with such realism that researchers are now turning to numerical model-derived data sets to diagnose the interplay between baroclinic, diabatic and turbulent proc-

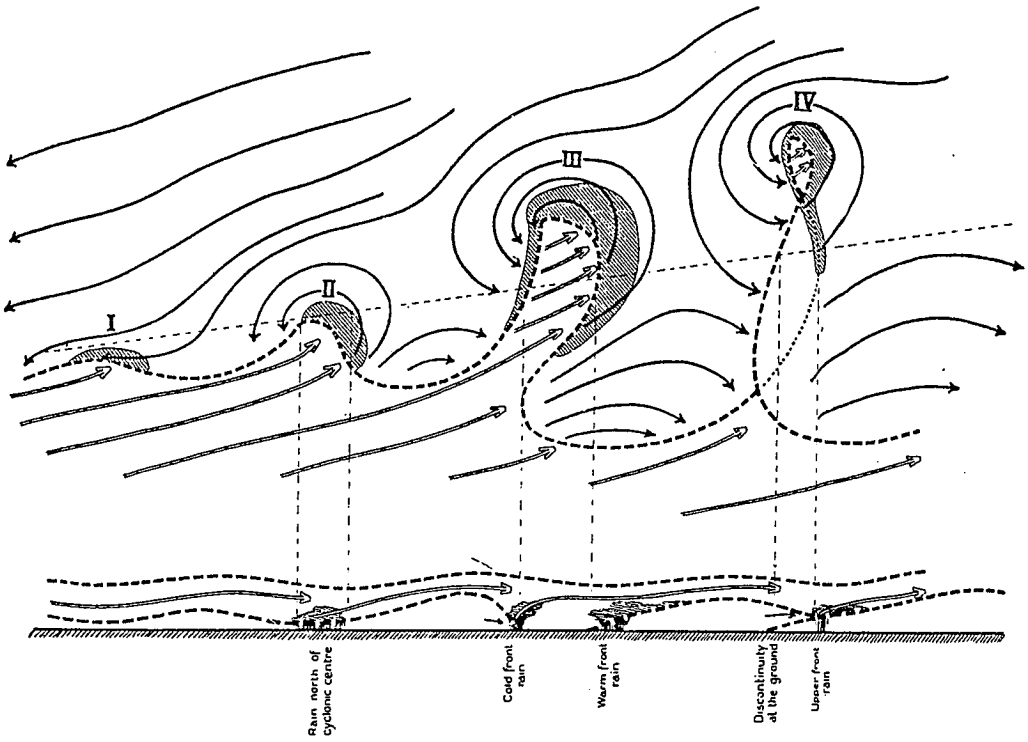

FIG. 10.12. The Norwegian frontal cyclone model (Bjerknes and Solberg 1922).

esses. This includes the evolution of fronts and jet streams and their associated circulations, precipitation systems and planetary boundary layer processes (e.g., Keyser et al. 1978; Keyser and Uccellini 1987; Whitaker et al. 1988; Kuo and Reed 1988; Kuo et al. 1990). In the following section, we present results from both numerical simulations and field studies which suggest some revisions to the Norwegian frontal-cyclone model.

10.4.1 Numerical Simulations

From the time of the early numerical studies of amplifying baroclinic waves (e.g., Edelmann 1963; Eliassen and Raustein 1968; Mudrick 1974), simulation experiments produced surface frontal configurations that differed markedly from those of the Norwegian frontal-cyclone model. The three-dimensional Eady (1949) wave simulations (e.g., Hoskins 1976; Hoskins and West 1979; Hoskins and Heckley 1981; Schär 1989) also produced unusual frontal configurations which the authors were hesitant to equate with those of the "real" atmosphere, since similar frontal structures had not yet been documented by synoptic meteorologists. Specifically, these studies showed heretofore undescribed frontal aspects such as (1) loss of cold frontal baroclinicity (frontolysis) near the cyclone center during the early phases of cyclogenesis, (2) the subsequent westward migration of warm frontal structure back into the northerly flow west of the intensifying cyclone and (3) the formation of a warm-core frontal seclusion in the post-cold-front cool air in the fully developed cyclone. Quite curiously, these simulations showed that the largest frontal baroclinicity during the cyclone life cycle occurred within the bent-back warm front to the rear (west) of the cyclone center. It should be noted that these controversial frontal evolutions were simulated with adiabatic models, excluding precipitation and surface boundary-layer processes.

As an example, the three-dimensional Eady-wave simulation by Schär (1989) showed the incipient cyclone developing along broad, zonal baroclinicity (Fig. 10.13a); the bridging of the contracting warm front across the cyclone center, together with cold-front contraction south of, but not in the vicinity of, the cyclone center (Fig. 10.13b); and, finally, the fully developed cyclone with its bent-back warm front and warm-core seclusion (Fig. 10.13c). Note that the warm-core seclusion contains lower temperatures than those initially within the warm sector of the cyclone.

We turn next to a numerical simulation of explosive extratropical marine cyclogenesis that was initialized with real data. The synoptic situation selected for this simulation was named for the Queen Elizabeth II (QE II) ocean liner, which was severely damaged by the fury of this North Atlantic storm. Synoptic discussions of the QE II cyclogenesis are presented in Gyakum (1983a,b) and Uccellini (1986). The present simulation was performed with a high-resolution version of the Penn State/NCAR regional numerical prediction model, documented by Anthes and Warner (1978), initialized at 12 UTC 9 September 1978. The grid resolution was 22.5 km in the horizontal and 15 layers in the vertical between the surface and 100 mb.

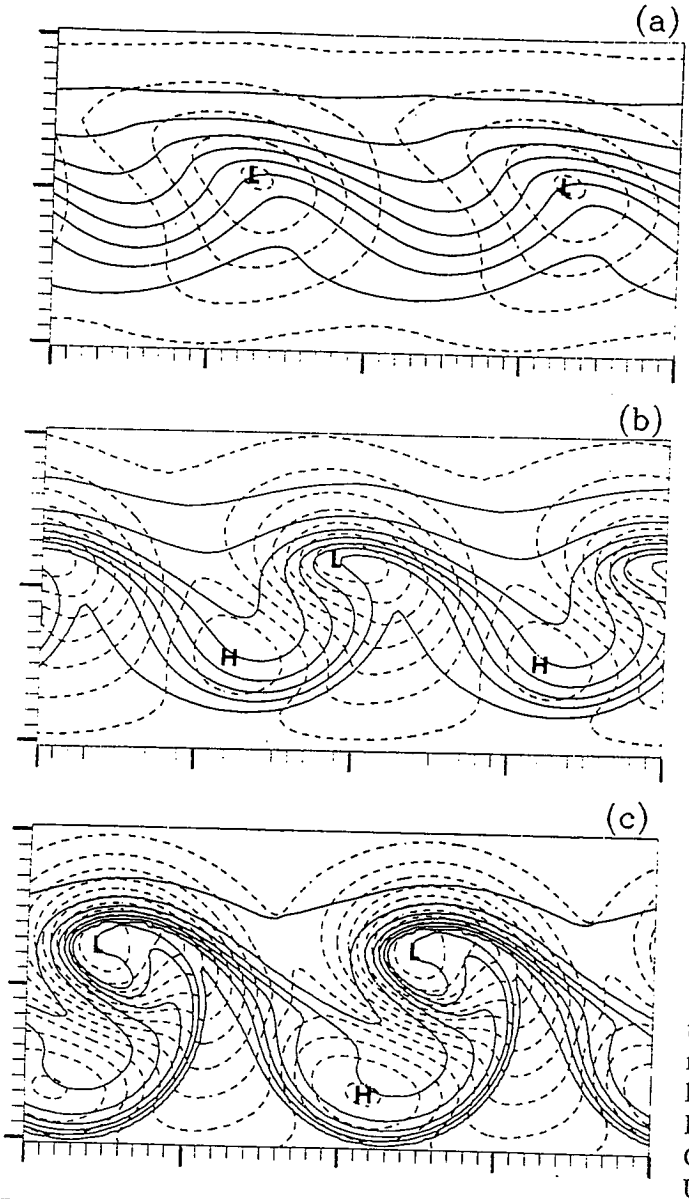

FIG. 10.13. Nonlinear semigeostrophic simulation of a baroclinic development from a small-amplitude disturbance to a cyclone. The diagrams show the surface fields of potential temperature (solid lines) and pressure (dashed lines) in a domain of 8000 × 4000 km. The contour interval is 2 K for potential temperature and 3 mb for pressure. The time interval between (a) and (c) is 96 h (Schär 1989).

Anthes et al. (1983) and Kuo et al. (1990) simulated the QE II cyclogenesis with coarser-resolution versions of the same model. In contrast to the Eady-wave simulations described above, the QE II simulations included boundary layer (air-sea interaction) and precipitation processes.

The high-resolution numerical simulation of the QE II cyclogenesis contained four phases of surface frontal evolution. The incipient cyclone (Fig. 10.14a) formed along a broad (~400 km wide) zonally continuous frontal zone. Twelve hours into the simulation (Fig. 10.14b) the previously continuous front had "fractured" near the center of the intensifying cyclone and the temperature gradients at the warm and cold front had contracted in width to ~100 km. As the cyclone continued intensifying at 18 hours (Fig. 10.14c), the cold front advanced eastward into the narrowing warm sector and the warm front developed westward (in storm-relative coordinates) such that frontogenesis was occurring in the northerly flow to the rear (west) of the cyclone within the cold polar air stream behind the advancing cold front. This phase of the cyclone-frontal evolution is termed the frontal "T-bone" because the advancing cold front had become oriented perpendicular to the "bent-back" extension of the warm front. At 24 hours, the time of maximum cyclone intensity (Fig. 10.14d), the cold front had advanced ~500 km east of the cyclone center and the bent-back warm front and cold polar air had cyclonically encircled the low center, entrapping a pocket of relatively warm air at its center. This warm-core "seclusion" formed within the baroclinicity of the polar air and did not involve air originating from the cyclone warm sector as in Phase IV of the Norwegian model (Fig. 10.12).

It is important to note that most, if not all, prior numerical simulations of both idealized and actual cases of extratropical cyclogenesis failed to reproduce the classical Norwegian cyclone-frontal occlusion. Instead we find, as in the above-described Eady-wave (Fig. 10.13) and QE II simulation (Fig. 10.14), that the warm-core seclusion within the polar air stream represents the final phase in the development of the cyclone. The question whether comparable structures are to be found in the real atmosphere is examined next.

10.4.2 Observational Studies

In their efforts toward advancing the understanding of the mesoscale structure of marine cyclones, researchers mounted extensive field observing programs which relied heavily upon meteorologically instrumented aircraft. Examples of the most recent of these field studies are the Genesis of Atlantic Lows Experiment (GALE) in 1986: U.S. East Coast cyclogenesis (see Dirks et al. 1988); the Alaskan Storm Program (ASP) in 1987: cyclogenesis in the eastern Pacific; and the Experiment on Rapidly Intensifying Cyclones over the Atlantic (ERICA) in 1988–89: western North Atlantic cyclogenesis (see Hadlock and Kreitzberg 1988). For the present illustration, we borrow results from forthcoming articles describing mesoscale evolutions during marine cyclogenesis observed during ASP and ERICA.

The first example of frontal evolution during extratropical marine cyclogenesis was documented with the NOAA P-3 aircraft over the central Pacific on 8–10 March 1987 during the ASP field study. This storm was observed with dropwindsonde and Doppler radar measurements in its T-bone phase (9 March) and fully secluded warm-core phase (10 March) of frontal evolution. The 1-km resolution visible satellite imagery (Fig. 10.15) shows three phases of cloud evolution during the life cycle of this cyclone: the cloud cluster associated with the initial incipient cyclone (Fig. 10.15a), the T-bone head and trailing

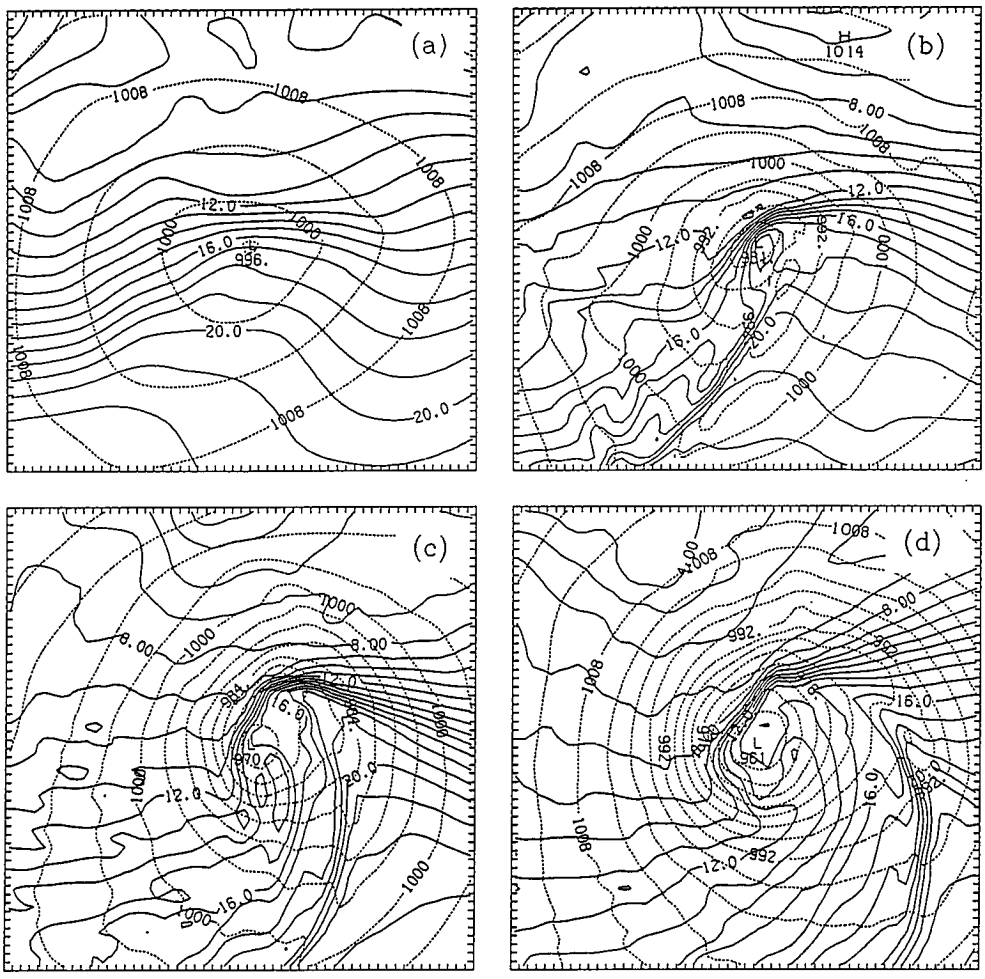

FIG. 10.14. Sea-level temperature (°C, solid lines) and sea-level pressure (mb, dashed lines) from a 24-h numerical simulation of the QE II marine cyclogenesis by the Penn State/NCAR regional model: (a) incipient frontal cyclone; (b) frontal fracture; (c) frontal T-Bone and bent-back warm front; (d) warm-core seclusion.

narrow cold-frontal rope cloud extending southwestward from the storm (Fig. 10.15b) and the fully developed cyclonic comma-shaped cloud signature of the warm-core seclusion (Fig. 10.15c).

The first NOAA P-3 flight into the developing cyclone originated from Adak, Alaska, an island on the Aleutian chain. Sixteen dropwindsondes were deployed from a pressure altitude of ~400 mb during a 5-hour period and space-time adjusted to ~00 UTC 9 March, given the phase velocity of the cyclone estimated from the satellite imagery. This analysis time is within 2 hours of the satellite cloud depiction in Fig. 10.15b.

The 850-mb temperature and geopotential height analysis and dropwindsonde wind vectors at ~00 UTC 9 March (Fig. 10.16) illustrate the frontal T-bone and bent-back warm front phase of this frontal cyclone. At this time, the sea-level pressure at the storm center, 963 mb, was ~20 mb lower than that 12 hours earlier as shown by the ECMWF analysis. The 850-mb temperature analysis was enhanced by incorporating cross-section analyses (discussed below). This analysis (Fig. 10.16) shows the east-west oriented warm front bridging across the cyclone center into the northerly flow west of the low. The north-south oriented cold-front baroclinicity extends southward from the warm front, forming the T-bone structure simulated in the previously discussed numerical studies (e.g., Fig. 10.14c). The 850-mb wind vectors illustrate the intensity of the storm circulation, as wind speeds exceeding 35 m s^{-1} were observed encircling the cyclone center during this phase of development.

Cross-section analyses of potential temperature and section-normal wind component were prepared along the projection lines AA′ and BB′ of Fig. 10.16. These analyses (Fig. 10.17a,b) intercept the warm front, and the cold front and bent-back warm front, respectively. The warm-front cross section (Fig. 10.17a) shows the front extending upward and northward, with the largest baroclinicity and vertical wind shear situated in the lower portion of the front near the sea surface. The second cross section (Fig. 10.17b) shows the cold front extending from ~400 mb down to the sea surface. The cold front was vertical below 700 mb in the vicinity of the "straight-up" convective cloud system situated at its leading edge. The cold-frontal convective cloud band was clearly evident in

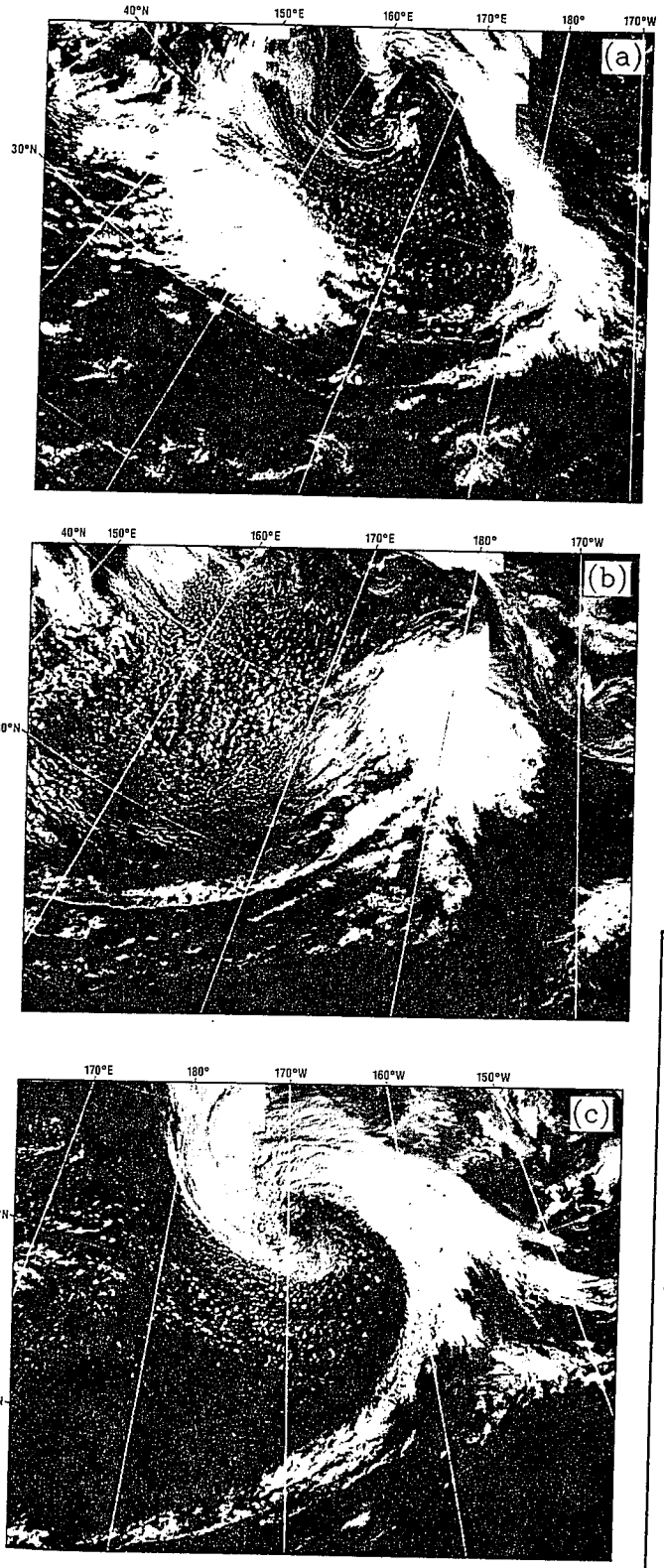

FIG. 10.15. 1-km resolution visible satellite images of three phases of cloud structure during the mid-Pacific cyclogenesis of 7–10 March 1987: (a) the cloud cluster (at left) of the incipient cyclone, 2045 UTC 7 March; (b) the bent-back warm frontal cloud head with the T-bone cold frontal convective cloud line and rope cloud trailing southwestward from the head, 2206 UTC 8 March; (c) the cyclonic spiral cloud signature of the mature cyclone and warm-core seclusion with deep mesoconvective cloud development within the warm sector in advance of the cold front, 2146 UTC 9 March.

the satellite cloud imagery (Fig. 10.15b). The vertical portion of the cold front and its narrow (~10 km) horizontal scale was also characteristic of the conceptualization of a convectively precipitating cold front (see Fig. 8.27) by Browning and Harrold (1970). The leading portion of the bent-back warm front is seen on the northern edge of the cross section.

The second flight into the cyclone originated from Anchorage, Alaska, ~24 hours after the first flight and deployed dropwindsondes to describe the warm-core seclusion phase of the cyclone life cycle. The 700-mb temperature and geopotential height analysis and wind vectors space-time adjusted to ~00 UTC 10 March 1987 (Fig. 10.18) clearly illustrate the −5°C warm-air seclusion (at its level of maximum baroclinicity), with the colder (−13°C) temperatures that cyclonically encircled the storm center along with the bent-back warm front. At this time, the storm central pressure was 973 mb, 10 mb higher than that documented from the aircraft 24 hours earlier, suggesting that cloud signatures such as that shown in Fig. 10.15c are indicative of the mature, and sometimes decaying, phase in the cyclone life cycle. A cross-section analysis of potential temperature and section-normal wind component (Fig. 10.19) was prepared along the projection line AA′ of Fig. 10.18. This analysis shows the vertical profile of the warm-core seclusion and the outward sloping baroclinicity of its encircling bent-back warm front. The

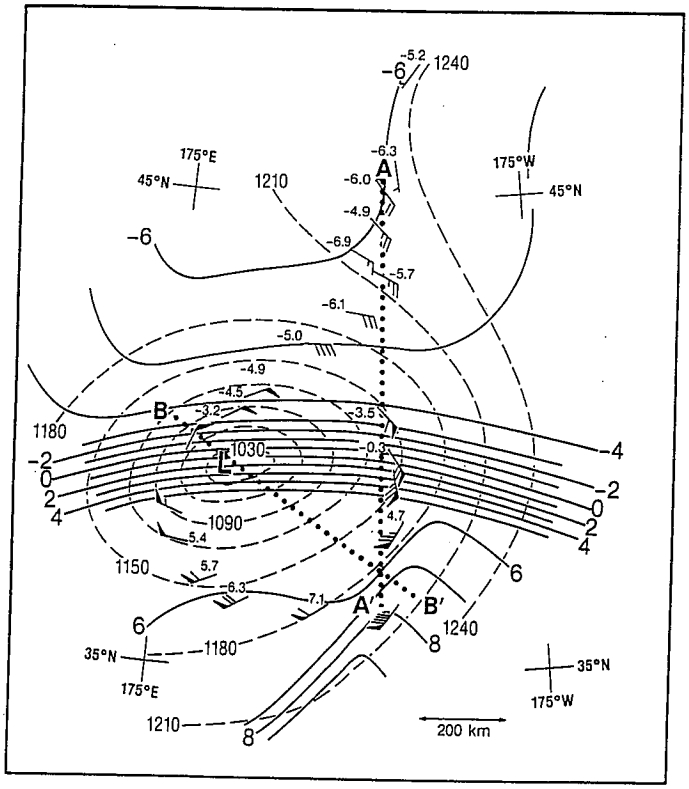

FIG. 10.16. 850-mb temperature (°C, solid lines) and geopotential height analysis (m, dashed lines) at ~00 UTC 9 March 1987, with dropwindsonde wind vectors and plotted temperatures. Lines AA′ and BB′ are cross section projections for Fig. 10.17a and b, respectively.

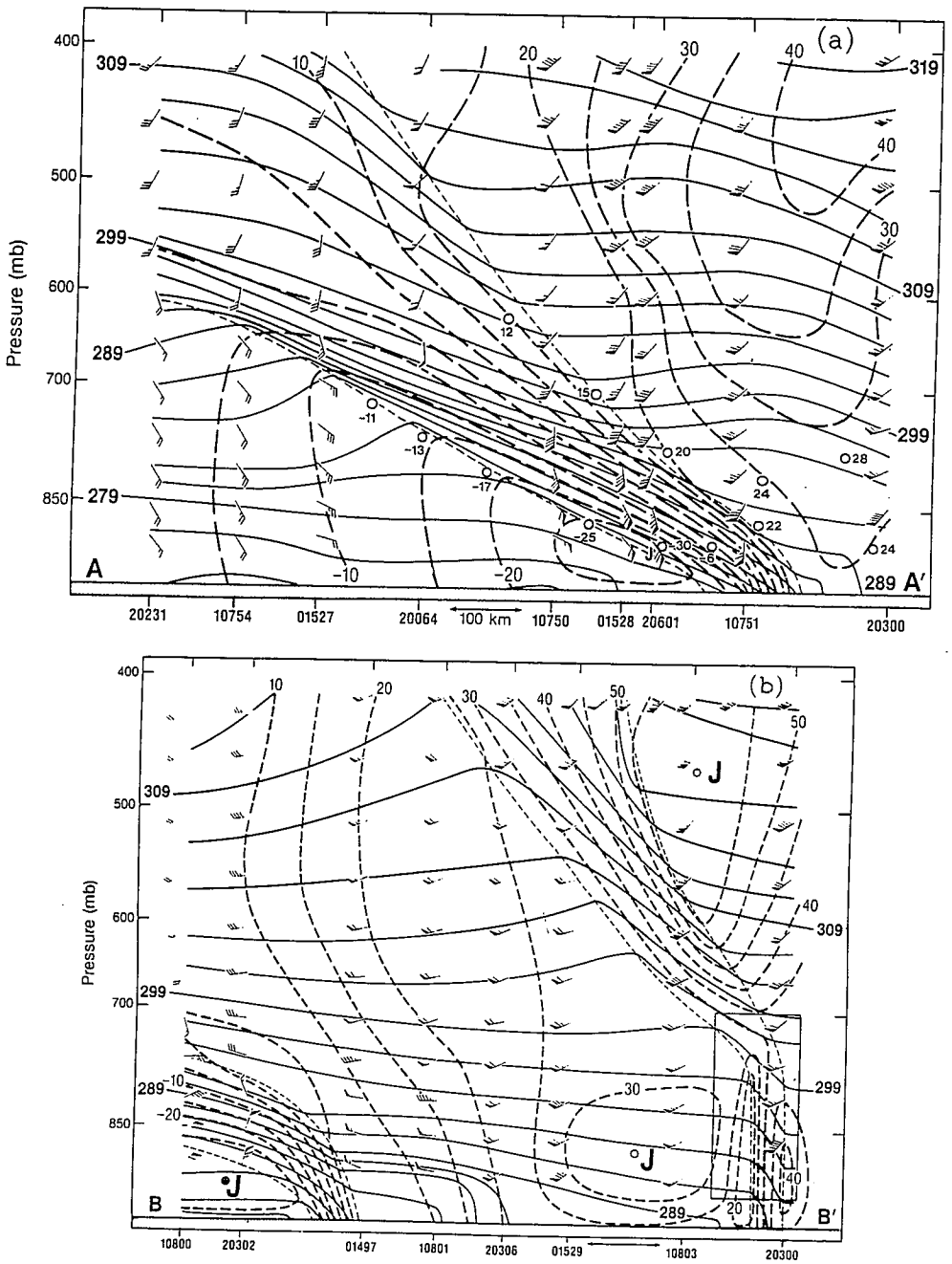

FIG. 10.17. (a) Cross-section analysis of potential temperature, section-normal wind component (m s^{-1}, heavy dashed lines) and frontal boundaries (thin dashed lines) along AA′ in Fig. 10.16. Flags and barbs show winds observed by dropwindsondes (numbered at bottom); Doppler radar wind observations, open circles with wind speeds beneath. (b) Section along line BB′ of Fig. 10.16. Positions of jet stream cores, J; inner boxed area indicates domain of Doppler radar wind observations.

highest wind speeds were found near the sea surface within the low-level jet on the cold side of the secluding front.

An excellent example of the frontal fracture and T-bone phase was observed during the pre-ERICA test flights made on 27 January 1988, one year prior to the full-scale field study. These observations were taken within a rapidly deepening cyclone that formed off the New Jersey coast, reaching its lowest central pressure (962 mb) over the Gulf of Saint Lawrence. This storm was observed with the NOAA P-3 research aircraft, the National Center for Atmospheric Research (NCAR) Loran dropwindsonde system and operational surface observations and eastern North American rawinsonde soundings. Results from this study are discussed in Neiman et al. (1990).

The 920-mb temperature and geopotential height analysis and wind vectors (Fig. 10.20) were derived from space-time adjustment of the aircraft observations to 12 UTC 27 January 1988, the time of the supporting operational upper-air soundings. The 920-mb temperature analysis shows the warm front extending across Nova Scotia, through the cyclone center, then turning southward as the bent-back warm front in the northerly flow west of

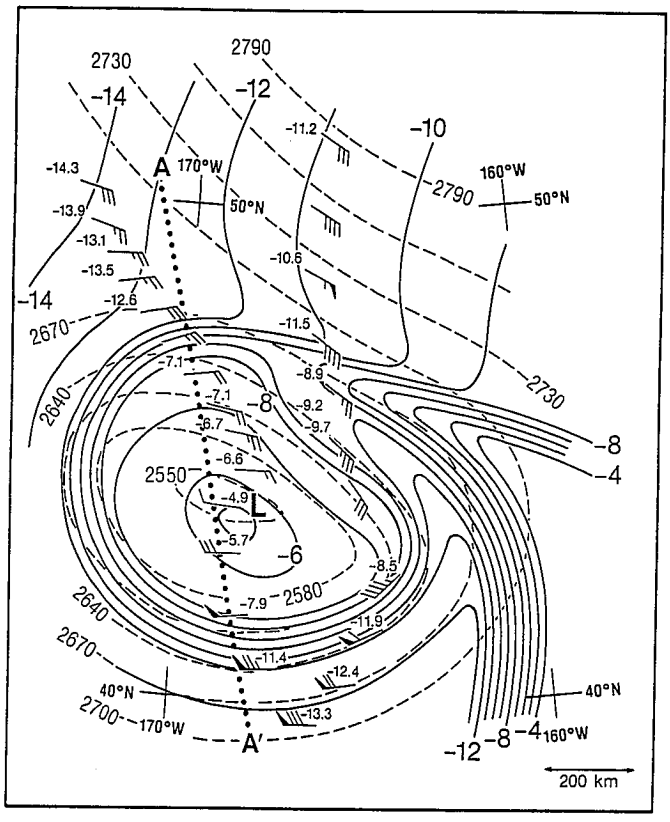

FIG. 10.18. 700-mb temperature (°C, solid lines) and geopotential height (m, dashed lines) analysis at ~00 UTC 10 March 1987, and wind vectors. Line AA', cross-section projection line for Fig. 10.19.

the storm center. The cold front was situated in the southerly flow east of the cyclone center and extended southward paralleling the East Coast of the U.S. At this time in the cyclone frontal evolution, the warm and cold fronts were distinctly disconnected (fractured), and the warm and cold frontal orientations had formed the above-described frontal T-bone configuration (e.g., Figs. 10.14c and 10.16).

The cross-section analysis of potential temperature and section-normal wind component (Fig. 10.21) along the projection line AA' of Fig. 10.20 intercepts the cold front and the bent-back warm front. The frontal structures within this analysis show the cold front sloping upward from the sea surface to the tropopause and its associated vertical and horizontal wind shear beneath the ~90 m s^{-1} polar jet stream at ~250 mb. The shallow bent-back warm front is seen within the cooler air west of the cold front, its warm boundary situated near the center of the cyclone.

Our final example of cyclone-frontal evolution is taken from the analysis of the ERICA field measurements of the extreme cyclogenesis event that occurred over the western North Atlantic on 4–5 January 1989. This storm was observed through its entire life cycle with five NOAA P-3 research flights, sea-surface drifting buoys and an enhanced eastern U.S. upper-air network. The central pressure of this storm decreased by 65 mb (to 935 mb) in 24 hours during its rapid development phase. The NOAA/GOES visible satellite image at 1631 UTC 4 January 1989 (Fig. 10.22) shows the dramatic cloud structure associated with the end of the period of maximum cyclogenesis. Note the large areal coverage of the storm cloud signature, extending meridionally from eastern Cuba to the south coast of Newfoundland (~5000 km) and zonally from the U.S. East Coast to halfway across the North Atlantic (~4500 km).

The second of three low-level flights into the cyclone documented the structure of the bent-back warm front and the cold front. By the mid-time of the flight (~17 UTC 4 January), nearly coincident with the time of Fig. 10.22, the storm central pressure had decreased to ~950 mb. The analysis of 300-m temperature and sea-level pressure and plotted 300-m wind vectors (Fig. 10.23) were prepared from aircraft flight-level and dropwindsonde observations space-time adjusted to 17 UTC. This analysis shows that the frontal evolution had progressed into its bent-back

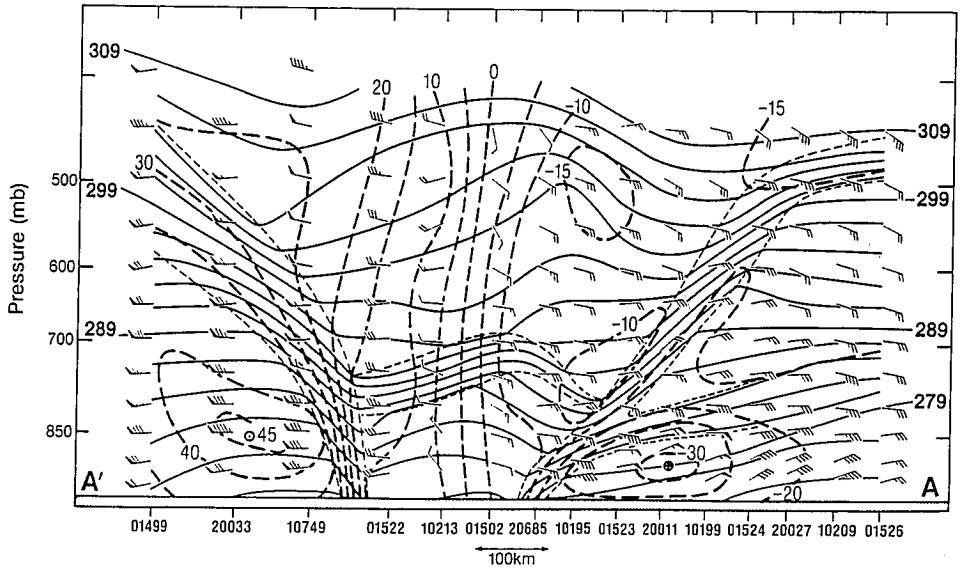

FIG. 10.19. As in Fig. 10.17, but for line AA' of Fig. 10.18.

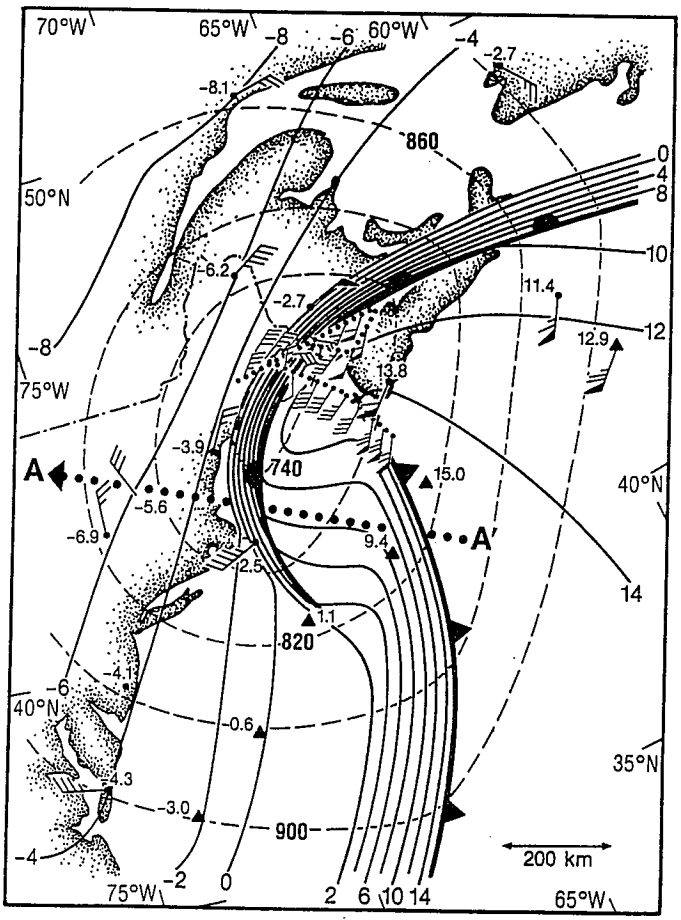

FIG. 10.20. 920-mb temperature (°C, solid lines) and geopotential height (m, dashed lines) analysis at ~12 UTC 27 January 1988. NOAA P-3 920-mb flight track, small-dotted lines with plotted wind vectors. Dropwindsonde deployment positions denoted by triangles. 920-mb temperatures plotted at rawinsonde and dropwindsonde positions. Warm and cold front boundaries indicated with conventional symbols. Line AA′, segment of cross-section projection line for Fig. 10.21.

face. The front broadened with height to ~50 km by 600 mb. A prefrontal mesoconvective cloud system was situated at the leading edge of the cold front and extended ~1500 km along the front as shown in the satellite image (Fig. 10.22).

The final low-level flight into the cyclone was made during the period of maximum storm intensity. At this time (~03 UTC 5 January), the storm central pressure had decreased to ~935 mb and its frontal evolution had progressed to the seclusion phase. The analysis of the 300-m temperature and sea-level pressure and plotted 300-m wind vectors space-time adjusted to ~03 UTC 5 January are presented in Fig. 10.25. The 300-m temperature analysis shows that the bent-back warm front and the cold polar air had almost completely encircled the cyclone center, secluding a mesoscale (~100 km) warm pocket of previously post-cold-frontal air near the low center. The seclusion temperatures were ~7 K warmer than those on the cold side of the encircling front. Wind speeds ~40 m s^{-1} were observed at the cold side of the frontal seclusion and the west-east distance across the seclusion, encircling wind speed maximum and cold air was ~140 km—truly mesoscale.

Cross-section analyses of potential temperature and section-normal wind components were prepared along the lines BB′ and AA′ of Fig. 10.25 to describe the vertical structure of the bent-back warm front and frontal seclusion, respectively. The warm-front cross section (Fig. 10.26a), constructed north of the cyclone center, shows the narrow (~50 km), shallow (~100 mb) bent-back warm front sloping upward and westward, overlying the ~40 m s^{-1} low-level (~900 mb) wind speed maximum within the marine boundary layer. This frontal structure is similar to that shown in the previous frontal analyses (Fig. 10.24). Note the shallowness of the strong northerly flow between 57° and 60°W (Fig. 10.26a) associated with warm front and cold frontal T-bone phase, as the warm front had developed west of the frontal triple point, through the cyclone center, and into the westerly flow to the south. The cold front had advanced ~300 km east of the cyclone center.

Cross-section analyses were prepared to describe the vertical structure of the bent-back warm front (Fig. 10.24a and b, along lines AA′ and BB′ of Fig. 10.23) and the cold front (Fig. 10.24c, along line CC′). The bent-back warm-frontal cross sections (Fig. 10.24a,b) show the strongest northeast to northerly wind speeds (~40 m s^{-1}) within the marine boundary layer beneath the front. The ~50 km width frontal zone exhibited mesoscale magnitudes of horizontal temperature gradient (~10 K/100 km), cross-frontal wind shear (~10^{-3} s^{-1}) and vertical wind shear (~40 m s^{-1}/100 mb). The cross-section analysis through the cold front (Fig. 10.24c) shows the extreme narrowness (~2 km) and sharpness of its gradients near the sea sur-

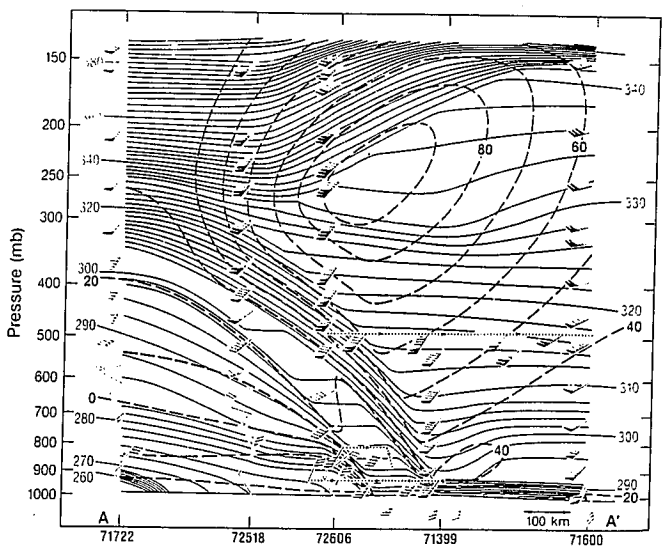

FIG. 10.21. As in Fig. 10.17, but for line AA′ of Fig. 10.20. NOAA P-3 flight track and wind vectors as in Fig. 10.20.

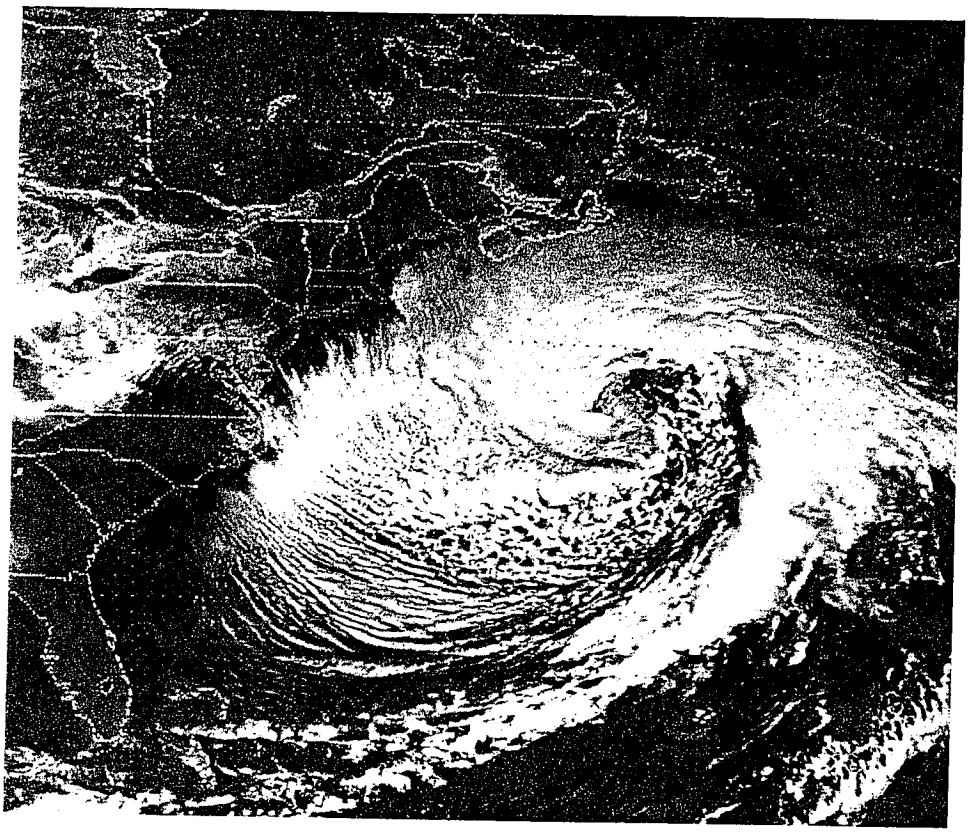

FIG. 10.22. 1-km resolution visible image at 1631 UTC 4 January 1989.

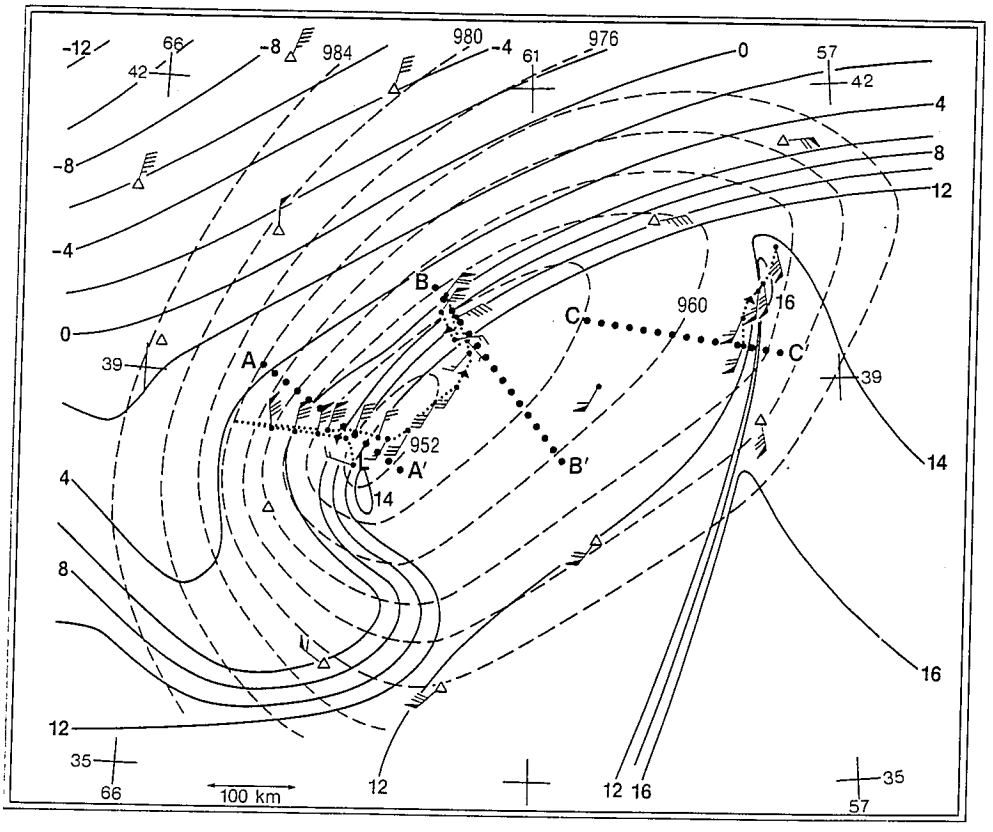

FIG. 10.23. 920-mb temperature (°C, solid lines) and sea-level pressure (mb, dashed lines) analysis at ~17 UTC 4 January 1989. Lines AA′ and BB′, and CC′ are cross-section projection lines for Fig. 10.24a, b and c, respectively. NOAA P-3 flight tracks, dropwindsondes and wind vectors as in Fig. 10.20.

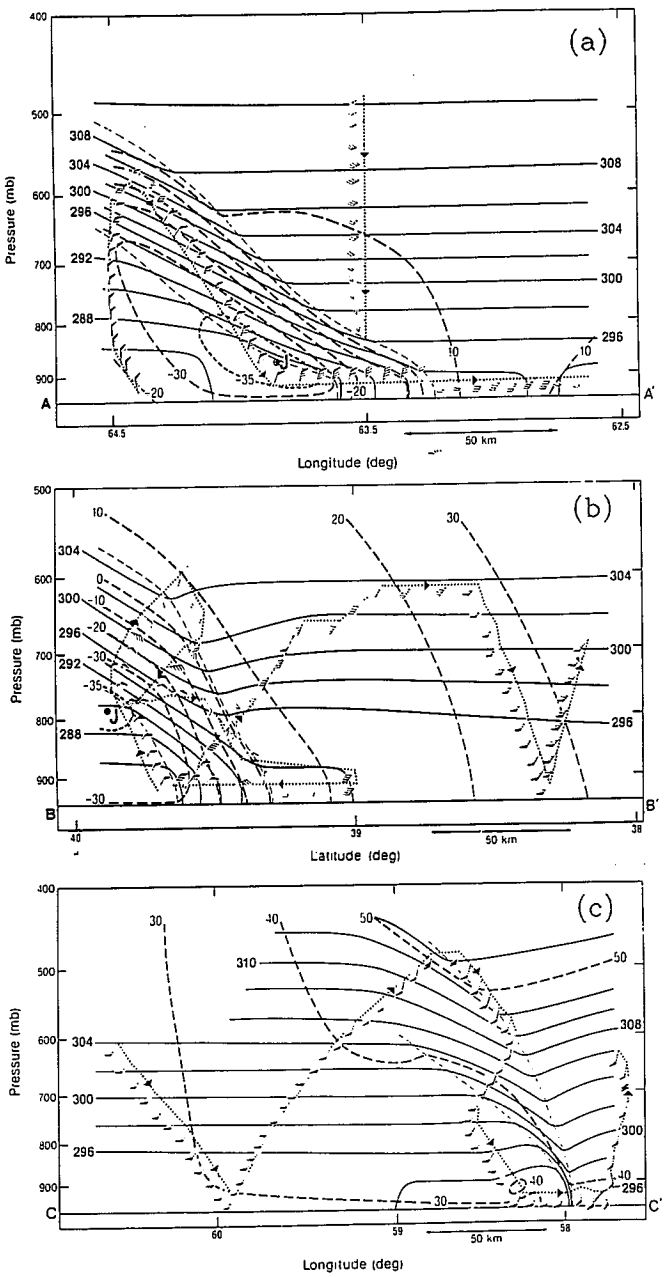

FIG. 10.24. Cross-section analyses of potential temperature (K, solid lines), section-normal wind component (m s^{-1}, dashed lines) and frontal boundaries along the lines AA′ (a), BB′ (b) and CC′ (c) of Fig. 10.23. NOAA P-3 flight track and wind vectors as in Fig. 10.20.

the reversal in wind direction to southerly above the frontal zone. The cross section across the warm-core seclusion and cyclone center (Fig. 10.26b) illustrates the intensity of the inner core of the mesoscale circulation near the cyclone center and the shallowness of the warm core structure. Maximum wind speeds in the northerly and southerly flows exceeded 35 and 50 m s^{-1}, respectively. The radius of maximum wind speed at 900 mb measured with respect to the center of the storm circulation was 75 km and increased with height to ≳ 200 km at 700 mb (~3 km). The baroclinicity of the encircling frontal zone sloped outward with height away from the cyclone center.

10.4.3 *A Conceptual Visualization of Cyclone-Frontal Evolution*

We conclude this section by integrating the findings of numerical and observational studies into a conceptual model of the structural evolution of surface fronts during the life cycles of extratropical cyclones. Before proceeding, it should be noted in retrospect that the essence of the frontal evolution described herein was realistically simulated with highly idealized representations of baroclinic flows (e.g., the three-dimensional Eady wave), suggesting that the simulated and observed frontal evolutions are primarily a manifestation of the horizontal deformations and associated vertical circulations within amplifying adiabatic baroclinic waves. Though precipitation and boundary-layer processes act to modulate the time scale and intensity of baroclinic waves and their internal fronts, research results to date suggest that the basic structural evolution of fronts within cyclones is driven by the adiabatic component of the motions.

The proposed conceptual model describing four phases of frontal structure during the life cycle of extratropical cyclones is presented in Fig. 10.27. The model incorporates the results of the previously described simulation and observational studies. The four phases of frontal evolution are: (1) the continuous and broad (~400 km across) front which represents the birthplace of the incipient frontal cyclone (Fig. 10.27I); (2) the frontal fracture in the vicinity of the cyclone center and scale contraction of the discontinuous warm and cold frontal gradients (Fig. 10.27II); (3) the frontal T-bone and bent-back warm front, characteristic of the midpoint of cyclogenesis (Fig. 10.27III); and (4) the warm-core seclusion within the post-cold frontal polar air stream representing the culmination of frontal evolution within the mature, fully developed cyclone (Fig. 10.27IV).

10.5 Future Directions

Having considered selected past and present interpretations of the structure and dynamics of fronts, jet streams and the tropopause, we conclude this chapter with our vision of future directions for advancing the understanding of these weather systems.

From the numerical modeling standpoint, relentless advances in supercomputer technology will shortly lead to regional-scale (~1000 × 1000 km) frontal and jet stream simulations with spatial grid resolutions capable of resolving individual cloud systems, boundary-layer circulations, internal frontal circulations such as gravity waves and shear instabilities, and moist and dry symmetric instabilities. These numerical models will have horizontal and vertical grid resolution ~1 km and ~100 m, respectively, with explicit rather than parameterized representations of "present day" small-scale motions (e.g., cumulus clouds, boundary-layer processes). There will be an entirely new spectrum of microscale processes to be considered, such as cloud microphysics.

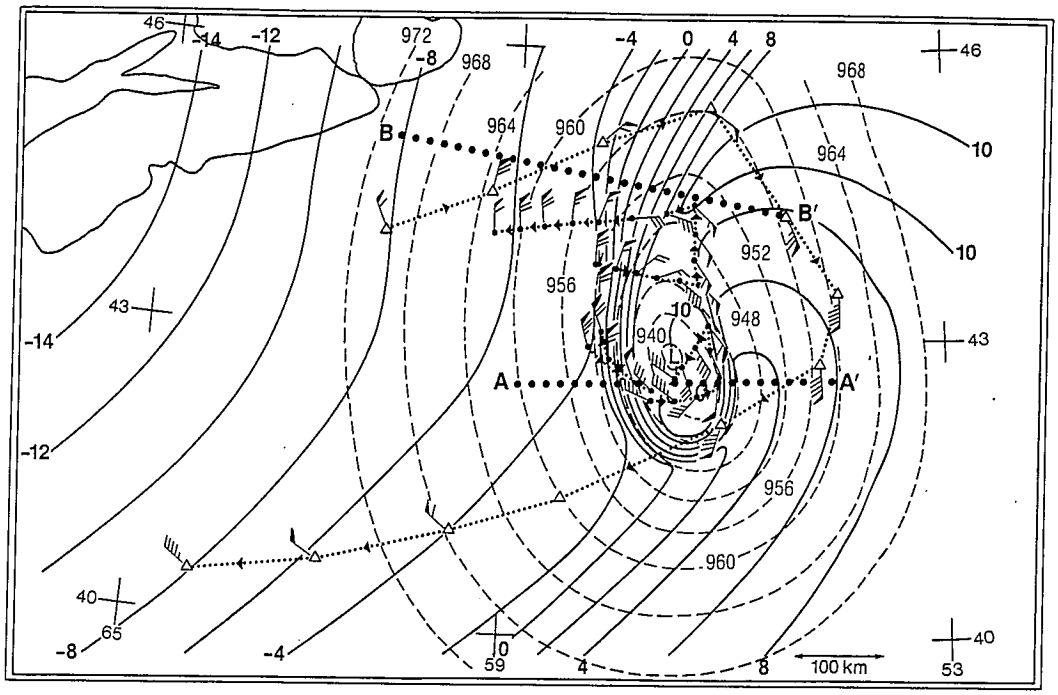

FIG. 10.25. 895-mb analysis of temperature (°C, solid lines) and sea-level pressure (mb, dashed lines) at ~03 UTC 5 January 1989. Lines BB′ and AA′ are cross-section projection lines for Fig. 10.26. Flight tracks, frontal boundaries, dropwindsondes and wind vectors as in Fig. 10.20.

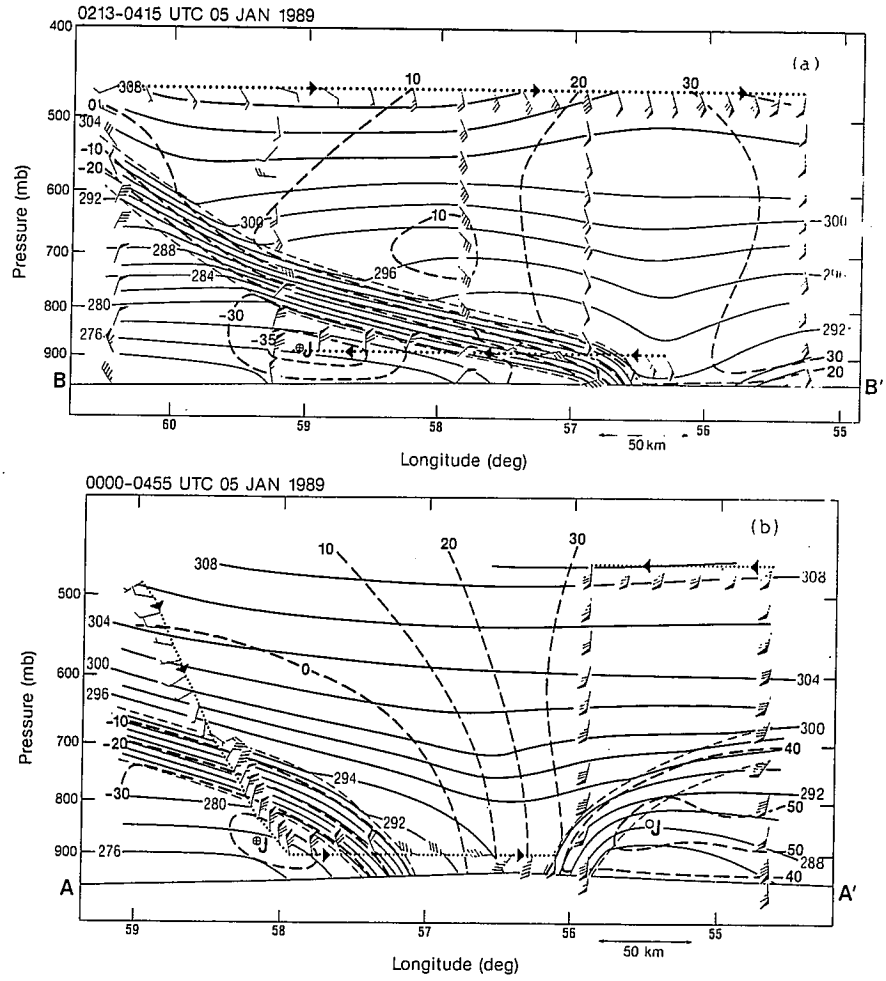

FIG. 10.26. Cross-section analyses of potential temperature (K, solid lines), section-normal wind component (m s^{-1}, heavy dashed lines) and NOAA P-3 flight track with wind vectors along lines BB′ (a) and AA′ (b) of Fig. 10.25. Dropwindsonde winds, vectors without connecting dotted lines.

These models will be used to simulate processes such as frontal-scale contraction from synoptic-scale (>500 km) gradients down to the nonhydrostatic microscale (<1 km), and the interaction of these sharp frontal gradients with precipitation systems and steep topography. The three-dimensionality of numerical models will facilitate the study of phenomena and processes such as mesoscale along-front variability, pre- and post-frontal boundary-layer circulations and their interaction with internal frontal circulations, interactions between fronts and mesoconvective (linear and cellular) precipitation systems, and the impact of physiographic boundaries formed by oceans (coastal and current), ice edges, snow, soil moisture and land use (e.g., forests, urban, agricultural).

By the early years of the 21st century, computing technology will have advanced to the point that microscale frontal-jet stream processes will be explicitly incorporated into global short-range (< 24 hour) through seasonal simulation and forecast models, including frontal interactions with coupled ocean circulation and interactive sea-state (fetch-dependent ocean roughness) models. The coupling of next-generation atmospheric chemistry models with the advanced regional- and global-scale meteorological models will advance the study and prediction of natural and anthropogenic trace constituent transport and chemical transformations. Of special interest will be a focus upon the fine-scale details of stratospheric-tropospheric exchange and associated chemical processes, including the role of mesoscale and microscale frontal circulations and their associated precipitation systems in the atmospheric chemistry cycle.

From the theoretical standpoint, future considerations will be directed toward extending the theory of fronts and jet streams beyond the limits of the adiabatic, three-dimensional semigeostrophic theory. This will lead to the development of less restrictive diagnostic equations that include accelerations in the ageostrophic rotational and irrotational motions and the effects of nonconservative physical processes (e.g., latent and sensible heating, turbulent mixing). It will also be necessary to determine the importance of internal wave motions (e.g., inertia-gravity waves) in governing the dynamic balance and in forcing vertical circulations in the vicinity of jet-stream frontal-zone systems, as well as to advance the theory of moist mesoscale baroclinic instability and its interaction with synoptic-scale baroclinic/barotropic instability.

Perhaps the greatest challenge to the science resides within the area of technological innovations in atmospheric and oceanographic observing systems. The forthcoming numerical and theoretical advances will require validation through actual observations of the phenomena under investigation. What is necessary are nearly spatially

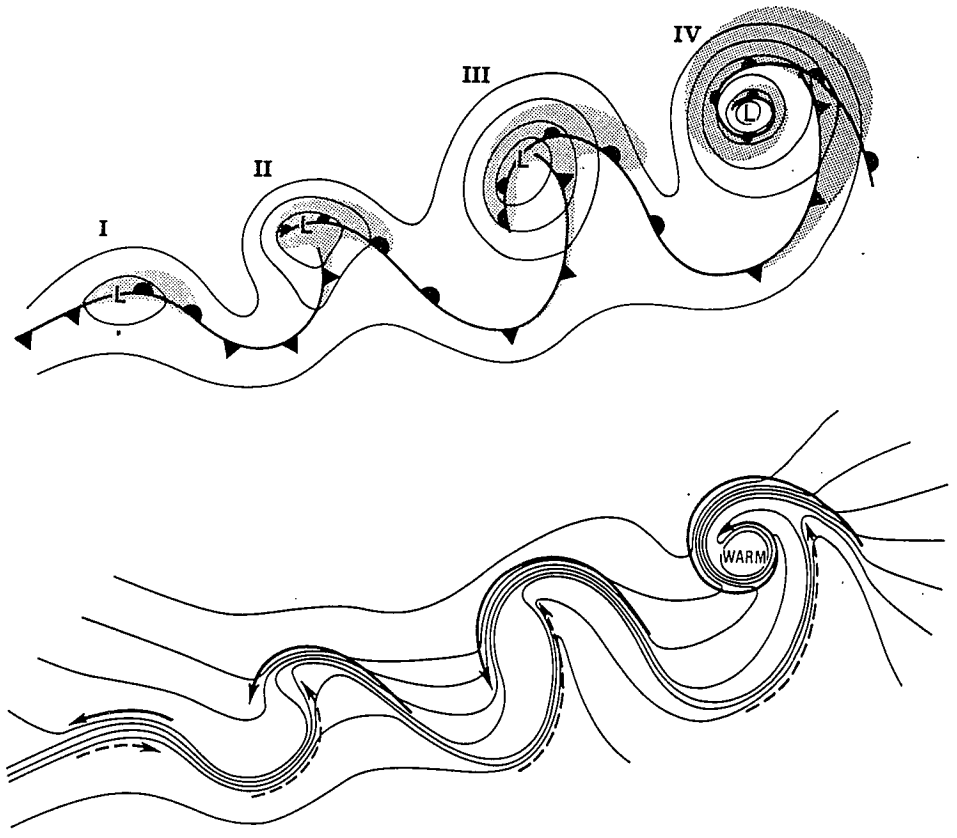

FIG. 10.27. The life cycle of the marine extratropical frontal cyclone: (I) incipient frontal cyclone; (II) frontal fracture; (III) bent-back warm front and frontal T-bone; (IV) warm-core frontal seclusion. Upper: sea-level pressure, solid lines; fronts, bold lines; and cloud signature, shaded. Lower: temperature, solid lines; cold and warm air currents, solid and dashed arrows, respectively.

and temporally continuous observations of all state parameters and velocity components, comparable in resolution to those from the next-generation numerical simulations. It is evident that the observing technology of the future must be of the remote sensing type, since limitations in the spatial and temporal resolutions of in-situ observing systems cannot satisfy the validation and initialization requirements of the simulation models.

Finally, it will be necessary to clarify the interplay between the mesoscale circulations and the synoptic-scale and planetary-scale motions. At the present time, there is considerable debate among researchers regarding the necessity of observing mesoscale weather systems in order to simulate and predict their impact upon larger-scale motions. Fronts, jet streams, mesoconvective systems, mountain waves and sea-breeze circulations have been simulated realistically with models initialized with synoptic-scale resolution data sets. This down-scale viewpoint suggests that mesoscale circulations are primarily a manifestation of the larger-scale motions and/or mesoscale physiography. An alternative viewpoint suggests that, under certain circumstances, upscale forcing by mesoscale phenomena and their associated processes can modulate the synoptic-scale through planetary-scale motions. The resolution of these differing interpretations regarding the interactions between the various scales of motion and their associated internal processes is a current focus of the science and should remain so well into the future.

Acknowledgments

The authors express their gratitude to Dr. N. Bond for providing the frontal analyses in Fig. 10.10a–c, to Ms. E. Donall for the numerical simulation exhibited in Fig. 10.14 and to Mr. P. Neiman for his assistance in preparing the analyses of marine cyclones shown in Section 10.4. We acknowledge Dr. Y.-H. Kuo and the NCAR Mesoscale and Microscale Meteorology Division for providing access to the NCAR/Penn State mesoscale prediction model and the NCAR computing facility. Special thanks are due to Mr. E. Hartnett, ERICA Data Center, Drexel University, for providing the data sets for the ERICA case studies presented herein, and to Prof. C. Kreitzberg, Drexel University, for encouraging our participation in the ERICA field program. We express our appreciation to the NOAA Office of Aircraft Operations and especially to the P-3 flight and engineering crews for their dedication in taking the observations presented in this chapter. Finally, the first author thanks the Office of Naval Research for support of the NOAA Alaskan Storm Program and Ocean Storms Program. The second author thanks the Office of Naval Research and National Science Foundation for supporting his effort in preparing this chapter through Contract N00014-88-K-0074 and Grant ATM-8721478, respectively.

We dedicate this chapter to the memory of Mrs. Mildred Birchfield of NOAA/WPL. Her superb technical assistance in preparing this and prior manuscripts has been invaluable, and she will be dearly missed.

REFERENCES

Abdullah, A. J., 1949: Cyclogenesis by a purely mechanical process. *J. Meteor.*, **6**, 86–97.

Anthes, R. A., and T. T. Warner, 1978: Development of hydrodynamic models suitable for air pollution and other mesometeorological studies. *Mon. Wea. Rev.*, **106**, 1045–1078.

——, Y.-H. Kuo and J. R. Gyakum, 1983: Numerical simulations of a case of explosive marine cyclogenesis. *Mon. Wea. Rev.*, **111**, 1174–1188.

Bergeron, T., 1928: Über die dreidimensional verknüpfende Wetteranalyse (I). *Geofys. Publ.*, **5**, No. 6, 1–111.

——, 1959: Methods in scientific weather analysis and forecasting. An outline in the history of ideas and hints at a program. *The Atmosphere and the Sea in Motion*, B. Bolin, Ed. Rockefeller Institute Press, 440–474.

Berggren, R., 1952: The distribution of temperature and wind connected with active tropical air in the higher troposphere and some remarks concerning clear air turbulence at high altitude. *Tellus*, **4**, 43–53.

Bjerknes, J., 1919: On the structure of moving cyclones. *Geofys. Publ.*, **1**, No. 1, 1–8.

——, 1932: Exploration des perturbations atmosphèriques à l'aide de sondages rapprochés dans le temps. *Geofys. Publ.*, **9**, No. 9, 1–52.

——, and E. Palmén, 1937: Investigations of selected European cyclones by means of serial ascents. *Geofys. Publ.*, **12**, No. 2, 1–62.

——, and H. Solberg, 1921: Meteorological conditions for the formation of rain. *Geofys. Publ.*, **2**, No. 3, 1–60.

——, and ——, 1922: Life cycle of cyclones and the polar front theory of atmospheric circulation. *Geofys. Publ.*, **3**, No. 1, 1–18.

Bosart, L. F., 1970: Mid-tropospheric frontogenesis. *Quart. J. Roy. Meteor. Soc.*, **96**, 442–471.

Browning, K. A., and T. W. Harrold, 1970: Air motion and precipitation growth at a cold front. *Quart. J. Roy. Meteor. Soc.*, **96**, 369–389.

Carbone, R. E., 1982: A severe frontal rainband. Part I: Stormwide hydrodynamic structure. *J. Atmos. Sci.*, **39**, 258–279.

Carlson, T. N., and F. H. Ludlam, 1968: Conditions for the occurrence of severe local storms. *Tellus*, **20**, 203–226.

——, S. G. Benjamin, G. S. Forbes and Y. F. Li, 1983: Elevated mixed layers in the regional severe storm environment: Conceptual model and case studies. *Mon. Wea. Rev.*, **111**, 1453–1473.

Charba, J., 1974: Application of gravity current model to analysis of squall-line gust front. *Mon. Wea. Rev.*, **102**, 140–156.

Defant, F., and H. Taba, 1957: The threefold structure of the atmosphere and the characteristics of the tropopause. *Tellus*, **9**, 259–274.

Dirks, R. A., J. P. Kuettner and J. A. Moore, 1988: Genesis of Atlantic Lows Experiment (GALE): An overview. *Bull. Amer. Meteor. Soc.*, **69**, 148–160.

Eady, E. T., 1949: Long waves and cyclone waves. *Tellus*, **1**, No. 3, 33–52.